

**SAE TECHNICAL
PAPER SERIES**

2002-01-0214

Cavitation Initiation, Its Development and Link with Flow Turbulence in Diesel Injector Nozzles

H. Roth

Imperial College of Science, Technology and Medicine, UK

M. Gavaises and C. Arcoumanis

City University, UK

**Reprinted From: Diesel Fuel Injection and Sprays 2002
(SP-1696)**

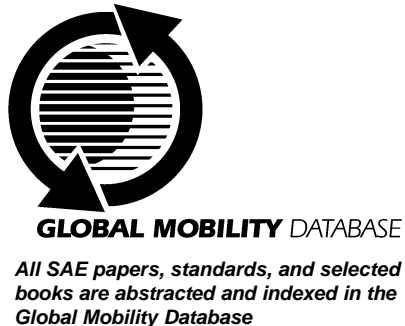


**SAE 2002 World Congress
Detroit, Michigan
March 4-7, 2002**

The appearance of this ISSN code at the bottom of this page indicates SAE's consent that copies of the paper may be made for personal or internal use of specific clients. This consent is given on the condition, however, that the copier pay a per article copy fee through the Copyright Clearance Center, Inc. Operations Center, 222 Rosewood Drive, Danvers, MA 01923 for copying beyond that permitted by Sections 107 or 108 of the U.S. Copyright Law. This consent does not extend to other kinds of copying such as copying for general distribution, for advertising or promotional purposes, for creating new collective works, or for resale.

Quantity reprint rates can be obtained from the Customer Sales and Satisfaction Department.

To request permission to reprint a technical paper or permission to use copyrighted SAE publications in other works, contact the SAE Publications Group.



No part of this publication may be reproduced in any form, in an electronic retrieval system or otherwise, without the prior written permission of the publisher.

ISSN 0148-7191
Copyright ©2002 Society of Automotive Engineers, Inc.

Positions and opinions advanced in this paper are those of the author(s) and not necessarily those of SAE. The author is solely responsible for the content of the paper. A process is available by which discussions will be printed with the paper if it is published in SAE Transactions. For permission to publish this paper in full or in part, contact the SAE Publications Group.

Persons wishing to submit papers to be considered for presentation or publication through SAE should send the manuscript or a 300 word abstract of a proposed manuscript to: Secretary, Engineering Meetings Board, SAE.

Printed in USA

2002-01-0214

Cavitation Initiation, Its Development and Link with Flow Turbulence in Diesel Injector Nozzles

H. Roth*

Imperial College of Science, Technology and Medicine, UK

M. Gavaises and C. Arcoumanis

City University, UK

Copyright © 2002 Society of Automotive Engineers, Inc.

ABSTRACT

The initiation and development of cavitation in enlarged transparent acrylic models of six-hole nozzles for direct injection Diesel engines has been visualised by a high-speed digital video camera in a purpose-built refractive index matching test rig. The obtained high temporal resolution images have allowed improved understanding of the origin of the cavitation structures in Diesel injector nozzles and clarification of the effect of sac geometry (conical mini-sac vs. VCO) on cavitation initiation and development in the nozzle holes. The link between cavitation and flow turbulence in the sac volume and, more importantly, in the injection holes has been quantified through measurements of the flow by laser Doppler velocimetry (LDV) at a number of planes as a function of the Reynolds and cavitation numbers. The anticipated enhancement of turbulence through the onset of cavitation was identified only at the entrance to the injection holes, with its effect most pronounced on the size of the developing cavitation bubbles and the homogeneity of the two-phase flow mixture at the nozzle hole exit.

INTRODUCTION

In many engineering applications, like core-cooling in a nuclear power plant, naval impeller systems, pump devices, or high pressure fuel injection systems, one encounters two-phase fluid flows where the occurring gas or vapour bubbles, representing the second phase in the flow, can have a significant influence on the liquid flow itself. Especially if the bubbly flow is in a cavitating state, knowledge about the dynamic behaviour of the bubbles and other cavitation structures is important in order to determine their impact on the performance of the equipment. For most of the hydraulic applications it is not desirable to have a cavitating flow within the machinery, since in these cases the collapse of cavitation bubbles can have an adverse effect on the mechanical integrity of the relevant components through surface

erosion [1, 2]. Secondly, the efficiency of the devices is reduced as a result of the lower overall density of the two-phase flow. Quite on the contrary, in engine fuel injection systems such as multi-hole Diesel injectors and in particular inside the injection nozzle holes, cavitation is recognised as offering advantages in the development of the fuel spray. This is due to the fact that the primary break-up and subsequent atomisation of the liquid fuel jet can be improved by the perceived enhanced turbulence caused by the cavitation patterns within the flow [3-7]. In addition, the dynamics of the cavitation bubbles in the nozzle holes are expected to enhance fuel atomisation through generation of smaller droplets which vaporise more rapidly, thus enhancing the fuel/air mixing and reducing ignition delay. Especially in the case of common rail injection systems operating with injection pressures up to 1500bar, the small dimensions of the nozzle holes can lead to extremely high flow velocities of the liquid fuel inside the holes (exceeding 400m/s). This fact encourages the different cavitation patterns to extend from their starting point around the hole inlet towards the hole exit where they influence the formation of the emerging spray [7-9]. The improved spray development then leads to a more complete combustion process, lower fuel consumption and reduced exhaust gas and particulate emissions.

In the above mentioned context, it is useful to examine the correlation between cavitation, which is present over a wide range of injection pressures and hence operating conditions, and the flow turbulence within the injector nozzle. Since flow investigations in real-size Diesel injectors are complicated due to their very small size, the high injection pressures and the high flow velocities, enlarged transparent models of Diesel injectors have been used for this work to allow for flow measurements to be obtained within the annulus, sac volume and injection holes of the nozzle under various flow conditions. By operating the large-scale nozzles at similar cavitation and Reynolds numbers to those found in real-size nozzles, dynamic flow similarity can be employed to ex-

* Currently visiting researcher at City University, London, UK.

trapolate the conclusions of the investigation in the large-scale model to the real-size injector [10].

Laser measurement techniques are capable of providing quantitative information about the local mean velocity and the turbulence intensity within the flow field provided that the flow area under investigation is large enough relative to the control volume of the laser beams. The refractive index matching technique, where both the acrylic nozzle and the working fluid have the same refractive index to allow the laser light to penetrate through the liquid-solid interfaces without distortion. In conjunction with laser Doppler velocimetry (LDV), sufficient optical access to the points of interest inside the nozzle can be obtained to allow reliable velocity measurements without the need for seeding particles under non-cavitating [11] or cavitating flow conditions.

Despite the important information gained from the LDV measurements, it is useful to have some insight in the actual formation and further development of the various cavitation patterns within the injection nozzle. Up to now it was common practice to obtain still images of the cavitating flow inside optically accessible injection holes (see review [12]). Previous work has revealed the basic structures of cavitation for a wide range of Reynolds and cavitation numbers, but failed to provide a dynamic picture of the developing pattern. Even with sequences of such images it was not possible to resolve the very rapidly developing cavitation inception. In this work, a digital high-speed video camera was employed together with the transparent enlarged models of various injection nozzles, making use of a refractive index matching flow rig under steady and quasi-transient flow conditions. In the case of the transient conditions, the needle position was fixed at different lifts and the flow rate was increased rapidly. This setup has allowed for sufficient temporal and spatial resolution in the video image sequences to identify the dynamic behaviour of all occurring cavitation structures under incipient and fully developed conditions.

EXPERIMENTAL WORK

REFRACTIVE INDEX MATCHING TEST RIG

Injection Nozzle Geometry

The transparent nozzles were manufactured from an acrylic material with a refractive index of 1.49. The dimensions of the enlarged nozzles and their needles represent a 20x magnification of Bosch six-hole vertical Diesel injection nozzles with conical mini-sac and valve covering orifice (VCO), respectively (Figure 1). Those types of nozzle geometries have their main difference in the way they seal off the high pressure region upstream of the needle seat from the injection holes. In the case of the conical mini-sac nozzle there is only a line contact between the needle and the needle seat which causes a relatively large amount of fuel to remain in the "dead volume" of the nozzle tip after the end of injection. In the

VCO nozzle there is virtually no sac volume left to be filled with fuel, since the needle is in surface contact with the needle seat and covers the injection holes completely. The nominal injection hole diameter of the enlarged models is 3.5mm which corresponds to a hole size of about 0.175mm in the real injector. To allow correspondence with the maximum lift of the first stage (0.08mm) and the second stage (0.3mm) of a real-size two-stage injector, the needle of the enlarged nozzles has been placed at the fixed lifts of 1.6mm and 6.0mm, respectively, throughout the measurement test matrix.

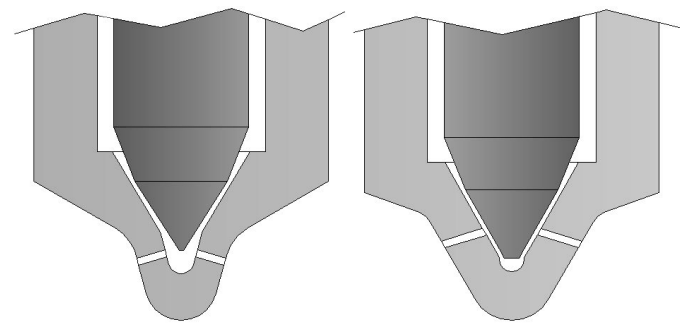


Figure 1: Geometry of the tip of the conical mini-sac type (left) and VCO type (right) injector

Working Fluid and Experimental Setup

The working fluid is a mixture of 32% by volume of Tetraline (1,2,3,4 - Tetrahydronaphthalene) and 68% by volume of oil of Turpentine in order to have a liquid that has the same refractive index as the acrylic nozzle and simulates closely the Diesel fuel properties. This refractive index matching method enables optical access without any distortion of light at the liquid-solid interfaces [13]. Therefore, imaging techniques and laser Doppler velocimetry can be applied satisfactorily [11].

A schematic overview of the experimental setup, enlarged injector and nozzle details is given in Figure 2 and Figure 3, respectively. The mixture was maintained at a temperature of $25 \pm 0.5^\circ\text{C}$ by a temperature controller, using a heater and cooler installed within the storage tank to keep the fluid refractive index at a level of 1.49. The flow rate of the mixture was controlled by a valve in the pipe downstream of the feed pump and measured by an orifice plate flow meter, calibrated to be accurate within 3%. Both injection and back pressures were adjusted by restricting the inflow and outflow of the injector, respectively. All pressures were recorded and are given in absolute values in the following tables. In order to reach sub atmospheric back pressures and therefore higher cavitation, CN, and Reynolds, Re, numbers, a suction pump was installed in addition to the main feed pump. To prevent the liquid from contact with air, which quickly leads to undesirable alterations of the physical properties of the working fluid, the spray development at the injection hole exit was not observed. Instead, the emerging liquid streams were collected in tubes and directed to the suction manifold to close the flow loop.

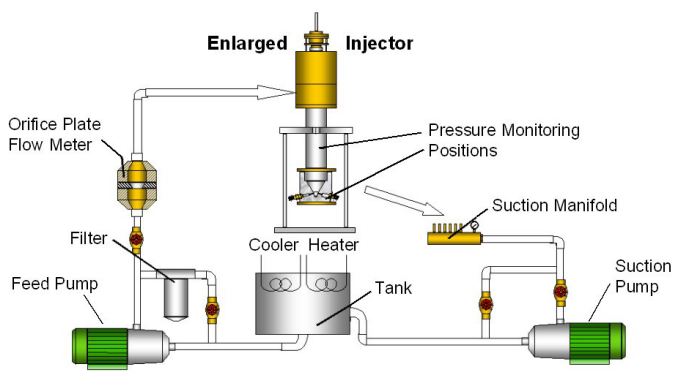


Figure 2: Schematic of refractive index matching test rig with closed flow loop

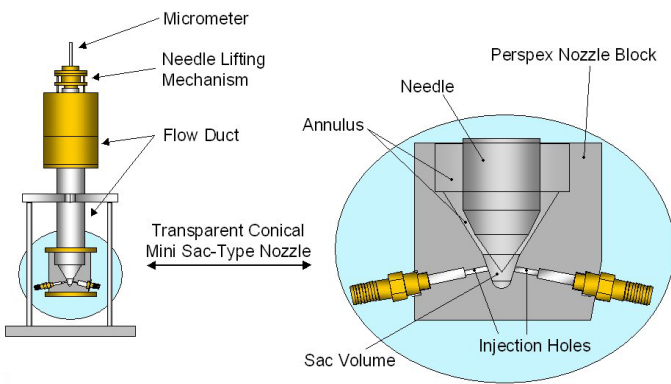


Figure 3: Enlarged injector and transparent model nozzle (in detail)

High-Speed Digital Video (HSDV)

Since the fuel flow through the injector nozzles, especially through the holes, is highly turbulent, all flow features can be expected to behave transiently and with short time-scales. This behaviour is virtually impossible to capture with still images, or an image sequence taken with a conventional CCD camera. Since it is important to gain knowledge about the dynamics of the cavitation inception and formation processes for various flow conditions and different nozzle geometries, a high-speed digital video system was set up together with the refractive index matching test rig in order to capture the cavitating injector flow inside the enlarged model nozzles. Figure 4 shows a schematic of the video system which was able to take up to 40,500 frames per second. A strong halogen floodlight together with some halogen spotlights were necessary to provide enough light for the non-intensified CCD video chip in combination with the high frame rates. The camera was triggered and controlled with the image processor unit via a remote control. In the image processor's memory the single video frames of one imaging sequence could be stored in digital form. From this memory it was possible to instantly replay the sequence of images, store the images with a VCR in PAL video format on a standard VHS tape, or transfer them to a PC via data cable. Once stored on the PC's hard disk, it was possible to create movie files from the single pictures of the same video sequence.

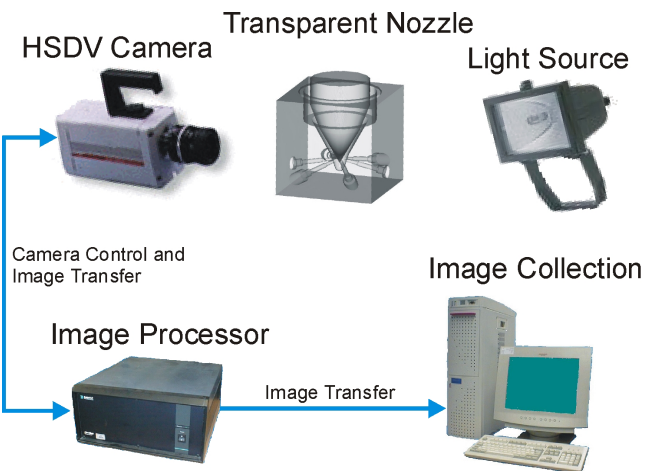


Figure 4: Schematic of the high-speed digital video imaging setup

LASER DOPPLER VELOCIMETRY

Experimental Setup

Figure 5 depicts the laser Doppler velocimetry (LDV) system which was set up around the transparent conical mini-sac type model nozzle of the refractive index matching rig.

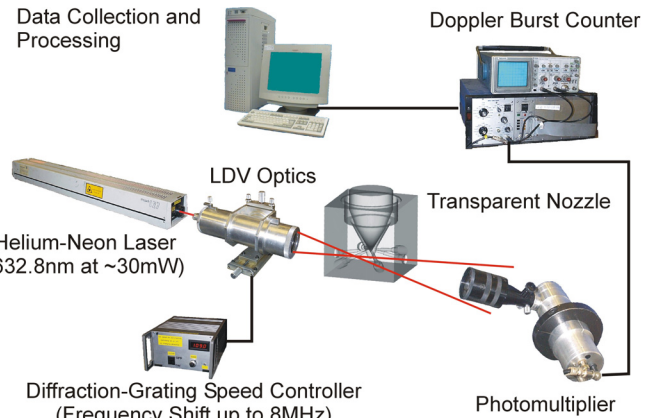


Figure 5: Schematic of the laser Doppler velocimetry setup

For the first series of measurements, the laser Doppler velocimeter comprised a Helium-Neon laser operating at a wavelength and power of 632.8nm and 30mW, respectively, a diffraction-grating arrangement to divide the laser beam into two beams of equal intensity with frequency shifts up to 8MHz, collimating and focusing lenses to bring the two beams to an intersecting volume, a photomultiplier and a frequency counter interfaced to a PC using a DMA board. Scattered light from the control volume by the crossing particles was collected with the photomultiplier and transformed into electrical signals which were processed by the Doppler burst counter. In this way the local mean velocities, V , and the root mean square, RMS, values for each measurement location within the flow field were obtained from a large number (>5000) of instantaneous velocity measurements. The local mean velocities are assembled from the probability

weighted, instantaneous velocities and the RMS values represent the square root of the probability weighted mean squares of the instantaneous velocity. For the second series of measurements the LDV setup had to be changed in order to allow for additional optical access and better signal to noise ratio. Therefore, the Helium-Neon laser was replaced with an Argon-Ion laser operating at 514.5nm wavelength and a power range of 100-600mW. The measurement locations were accessed from below using a laser mirror and the scattered light was collected sideways due to the new arrangement.

Measurement Locations and Conditions

The measurement locations were spread over the annulus, the sac volume and one injection hole on a central vertical plane passing through the axis of two injection holes facing each other. In Figure 6 and Figure 7 the lower part of the nozzle is shown, cut along the central vertical plane, and it is depicted where the horizontal and vertical velocity profiles were taken. There are horizontal planes located at $z = 4.5, 8.9, 11.0, 12.7, 14.5, 16.2, 19.0$ and 25.0mm above the lowest point of the sac volume and there are vertical planes located at $x = 6.2, 7.0, 8.5, 9.5, 10.5, 13.5$ and 16.5mm from the axis of symmetry of the nozzle.

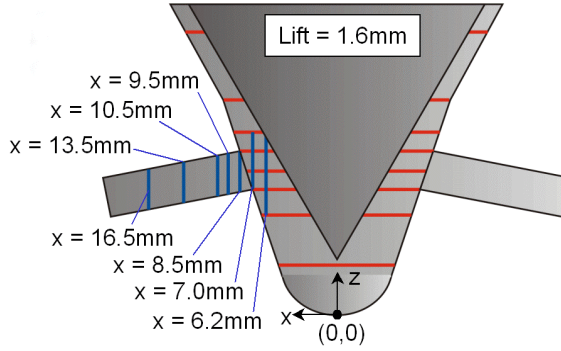


Figure 6: Vertical measurement planes in the conical mini-sac type nozzle

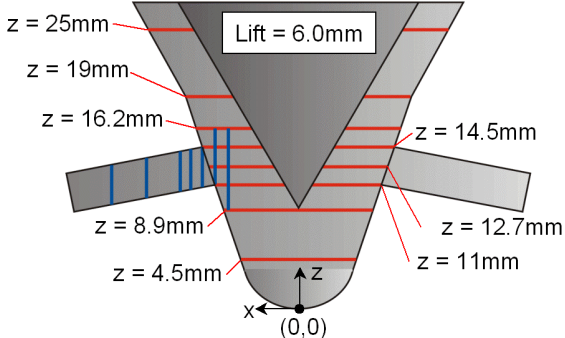


Figure 7: Horizontal measurement planes in the conical mini-sac type nozzle

For the first series of measurements one non-cavitating reference flow condition (highlighted in Table 1) was chosen in order to have a complete set of data describing the flow field in detail for all measurement planes.

This enables validation of the in-house 3-D CFD code with the obtained velocity data for the non-cavitating flow. Additional measurements at all conditions listed in Table 1 were concentrated in the injection hole along the planes $x = 9.5, 10.5$ and 13.5mm in order to obtain knowledge about the correlation between hole cavitation and turbulence intensity within the injection hole.

Needle Lift = 1.6mm			Needle Lift = 6.0mm		
Re	p_{inj} [bar]	p_{back} [bar]	Re	p_{inj} [bar]	p_{back} [bar]
0.37	2.70	2.00	0.34	2.05	1.56
0.44	2.55	1.80	0.45	1.80	1.27
0.70	1.90	1.16	0.50	1.75	1.20
1.05	1.60	0.83	0.83	1.40	0.81

Table 1: Flow conditions for the first series of LDV measurements; p_{inj} is the absolute injection pressure measured upstream of the nozzle, p_{back} is the absolute back pressure measured after the hole exit. The first two flow conditions for each needle lift setting are non-cavitating as reference.

The second series of measurements included flow conditions at increased cavitation and Reynolds numbers (Table 2) and additional measurement locations in the injection hole further downstream ($x = 16.5\text{mm}$). Some representative measurements were carried out inside the sac volume and at the entrance to the injection hole for high needle lift and varying cavitation numbers (conditions from Table 1, needle lift = 6.0mm) to determine the potential influence of cavitation on turbulence intensity.

Needle Lift = 1.6mm					
CN	Re	p_{inj} [bar]	p_{back} [bar]	U_{ini} [m/s]	Flow Rate [l/s]
0.44	18000	2.55	1.80	8.43	0.487
1.48	26800	2.80	1.19	12.58	0.726
2.39	33200	4.00	1.25	15.56	0.898
5.50	33400	4.00	0.70	15.66	0.904
Needle Lift = 6.0mm					
CN	Re	p_{inj} [bar]	p_{back} [bar]	U_{ini} [m/s]	Flow Rate [l/s]
0.45	21000	1.80	1.27	9.84	0.568
1.09	30200	2.40	1.20	14.15	0.817
1.48	34100	3.00	1.27	15.97	0.922
4.57	39500	4.00	0.80	18.50	1.068

Table 2: Flow conditions for the second series of LDV measurements. The first condition for each needle lift setting is non-cavitating for reference purpose.

In order to have confidence in the measured local mean velocities, a cross check with the flow rate through the nozzle was performed. The result for the flow rate from the calibrated orifice plate flow meter agreed within 2.5% with the flow rate obtained from the LDV velocity profiles integrated over the top annulus of the nozzle.

EXPERIMENTAL RESULTS

FLOW VISUALISATION

In order to better understand the dynamic behaviour of the various cavitation structures under different conditions, the refractive index matching test rig with the transparent model nozzles was operated at varying needle lifts and flow conditions (Tables 3 - 5) and the cavitating flow was visualised with the high-speed camera (Figure 4). The imaging area included all six injection holes, the lower part of the nozzle annulus and the volume around the needle tip.

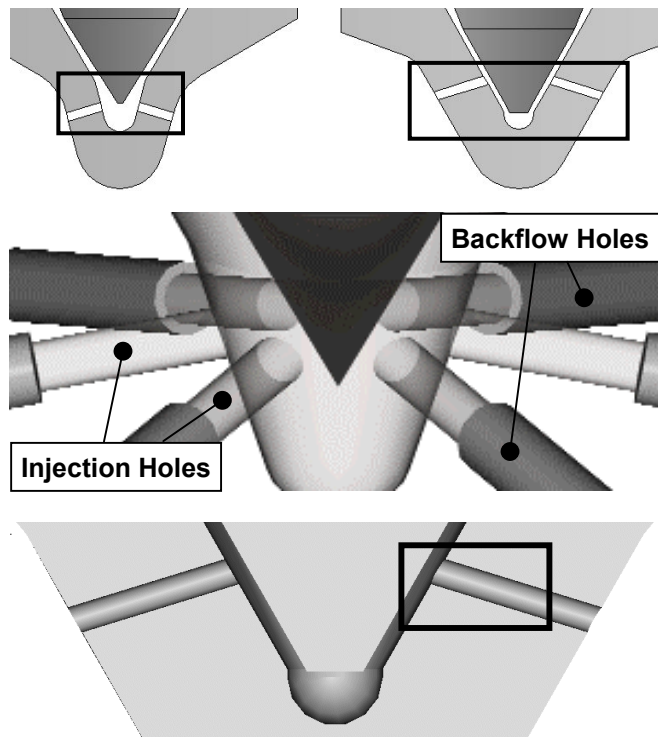


Figure 8: Schematic of the imaging areas and view points for high-speed digital video visualisation of all six injection holes (middle) in the conical mini-sac and VCO type nozzle and the one-hole close-up for the VCO type nozzle (bottom)

Figure 8 shows a schematic of the imaging area for the mini-sac and VCO nozzle where the dark triangle in the middle picture represents the needle tip. Both the outline of the needle tip and sac volume are hardly visible in the video image sequences shown further below due to the matching refractive index of the liquid and the acrylic nozzles. The six injection holes of the acrylic model nozzles are extended by larger diameter backflow holes which collect the emerging fuel and direct it towards the backflow tubes (not shown here). In order to visualise the cavitating flow through the holes "behind" those at the side and the volume between the needle and the needle seat, it was necessary to position the video camera at an angle. In addition to the imaging area described above, a close-up of one injection hole in the VCO type nozzle provided a more detailed view of the dynamic cavitation patterns. The schematic of that

close-up imaging area is shown in the lower picture of Figure 8.

Needle Lift = 1.6mm						
CN	Re	P _{inj} [bar]	P _{back} [bar]	U _{inj} [m/s]	Flow Rate [l/s]	Frame Rate [1/s]
0.70	17987	1.90	1.16	8.43	0.487	9000
1.05	17987	1.60	0.83	8.43	0.487	9000
1.48	26844	2.80	1.19	12.58	0.726	9000
2.39	33210	4.00	1.25	15.56	0.898	9000
5.50	33431	4.00	0.70	15.66	0.904	9000
Needle Lift = 6.0mm						
CN	Re	P _{inj} [bar]	P _{back} [bar]	U _{inj} [m/s]	Flow Rate [l/s]	Frame Rate [1/s]
0.50	21004	1.75	1.20	9.84	0.568	9000
0.83	21004	1.40	0.81	9.84	0.568	9000
1.09	30195	2.40	1.20	14.15	0.817	9000
1.48	34085	3.00	1.27	15.97	0.922	9000
4.57	39482	4.00	0.80	18.50	1.068	9000

Table 3: Flow conditions in the conical mini-sac type nozzle for high-speed digital video imaging of all six injection holes; p_{inj} is the absolute injection pressure measured upstream of the nozzle, p_{back} is the absolute back pressure measured after the hole exit.

Needle Lift = 1.6mm						
CN	Re	P _{inj} [bar]	P _{back} [bar]	U _{inj} [m/s]	Flow Rate [l/s]	Frame Rate [1/s]
0.81	16270	2.00	1.15	7.62	0.440	9000
1.02	17987	2.20	1.14	8.43	0.487	9000
1.52	23948	2.80	1.17	11.22	0.648	9000
2.48	29704	4.00	1.22	13.92	0.803	18000
5.50	29951	4.00	0.70	14.03	0.810	18000
Needle Lift = 4.0mm						
CN	Re	P _{inj} [bar]	P _{back} [bar]	U _{inj} [m/s]	Flow Rate [l/s]	Frame Rate [1/s]
0.71	23009	1.90	1.15	10.78	0.622	9000
0.94	27918	2.20	1.18	13.08	0.755	9000
1.58	34085	3.20	1.30	15.97	0.922	18000
2.00	38348	4.00	1.40	17.97	1.037	18000
5.00	38539	4.00	0.75	18.06	1.042	18000
Needle Lift = 6.0mm						
CN	Re	P _{inj} [bar]	P _{back} [bar]	U _{inj} [m/s]	Flow Rate [l/s]	Frame Rate [1/s]
0.60	23326	1.80	1.16	10.93	0.631	9000
0.77	26568	2.05	1.20	12.45	0.719	9000
1.07	32313	2.60	1.31	15.14	0.874	18000
1.71	38348	3.60	1.39	17.97	1.037	18000
4.34	40220	4.00	0.83	18.85	1.088	18000

Table 4: Flow conditions in the VCO type nozzle for high-speed digital video imaging of all six injection holes; p_{inj} is the absolute injection pressure measured upstream of the nozzle, p_{back} is the absolute back pressure measured after the hole exit.

The flow conditions examined in terms of flow rates and pressures cover the equivalent range from low to medium load of a real-size production injector used in passenger car Diesel engines. The needle lift positions of 1.6mm and 6.0mm correspond to the needle lift at the

first (0.08mm) and second stage (0.3mm) of a two-stage production injector.

Needle Lift = 1.6mm						
CN	Re	P _{inj} [bar]	P _{back} [bar]	U _{inj} [m/s]	Flow Rate [l/s]	Frame Rate [1/s]
0.81	16270	2.00	1.15	7.62	0.440	9000
1.02	17987	2.20	1.14	8.43	0.487	9000
1.52	23948	2.80	1.17	11.22	0.648	9000
Needle Lift = 4.0mm						
CN	Re	P _{inj} [bar]	P _{back} [bar]	U _{inj} [m/s]	Flow Rate [l/s]	Frame Rate [1/s]
0.71	23009	1.90	1.15	10.78	0.622	9000
0.94	27918	2.20	1.18	13.08	0.755	9000
1.58	34085	3.20	1.30	15.97	0.922	9000

Table 5: Flow conditions in the VCO type nozzle for close-up high-speed digital video imaging of one injection hole; p_{inj} is the absolute injection pressure measured upstream of the nozzle, p_{back} is the absolute back pressure measured after the hole exit.

Cavitation Pattern

As shown in previous studies investigating nozzle cavitation, this phenomenon initiates in areas of low local pressure [4, 9, 11]. Usually, these areas are found in the core of the recirculation zones formed at the upper corner of the injection hole inlet. The results in the large-scale mini-sac type nozzle revealed that increasing the cavitation number resulted in formation of different cavitation hole flow regimes [14, 15]. Initially a bubbly flow structure was identified (incipient cavitation) which consists of small bubbles easily recognisable since the cloud is not very dense and the bubble sizes seem to be relatively uniform. With increasing cavitation number the bubble clouds become more opaque and it is not possible any more to distinguish between individual bubbles. Moreover, the increasing coalescence of cavitation bubbles forms larger voids which lead to local vapour films (pre-film stage cavitation). A further increase of the cavitation number causes the flow to fully separate at the upper half of the nozzle hole inlet. This induces the formation of a vapour film type cavitation (film stage cavitation) where the relatively thin film follows the curved shape of the hole. These geometrically-induced cavitation patterns were found not to depend on the Reynolds number (flow rate), but the development of the cavitation structures was strongly affected by the cavitation number and both needle lift and needle eccentricity, in agreement to [16].

In addition to hole cavitation, string-type cavitation structures were observed to form in the holes and well inside the sac volume in areas where the pressure is expected to be almost equal to the higher upstream pressure (see also [9, 17]). Although the geometry of the examined nozzles is axisymmetric, a cross flow was observed linking one side of the sac volume to the other side while a vortex structure was identified to be present in the volume between needle, needle seat and two adjacent

holes. Figure 10 shows the nozzle flow and a few large air bubbles which were added to the liquid upstream of the nozzle in order to better visualise this flow structure. The vortex and string formation was attributed to the interaction between the high momentum annulus flow and the cross flow, which occurs due to the intermittent throttling of individual holes by already existing recirculation zones, or cavitation in the holes. As a result, the flow conditions at the vortex core lead to the formation of a low pressure region and, subsequently, of cavitation bubbles which coalesce immediately to a continuous vapour string.

Figure 9 shows representative images of cavitation strings which generally develop transiently and periodically between adjacent holes. The parts of the vortices being sucked into the hole inlet diffuse to large conical clouds of bubbles which then mix with the film cavitation structures further downstream.

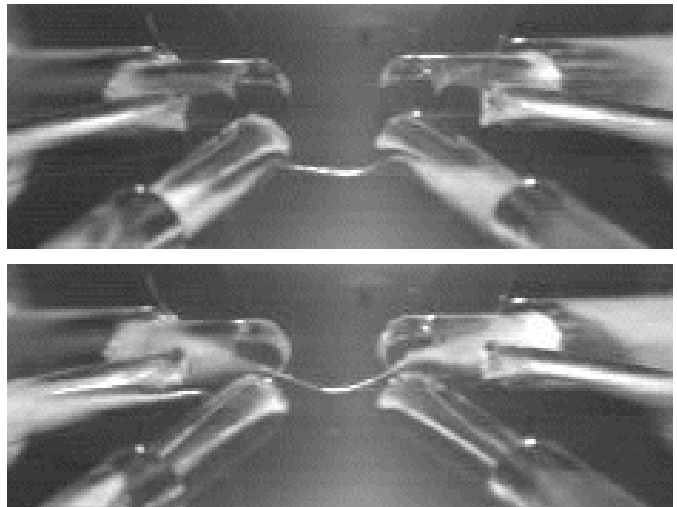


Figure 9: Cavitation strings each connecting two adjacent injection holes in the mini-sac type nozzle with needle lift = 6.0mm and CN = 4.57; The strings disintegrate into a cone of bubbles after entering the holes. This mist of bubbles mixes with the film type cavitation further downstream.

Besides the ‘hole connecting strings’ another form of string cavitation was identified quite frequently in the VCO type nozzle but less frequent in the mini-sac type nozzle; these to be referred to as ‘needle strings’. They appear to originate on the needle surface facing an injection hole inlet and extend downstream into the hole (Figure 11 and Figure 12). This is believed to be attributed to the strong vortex flow around the hole axis which leads to the above described string formation process due to the low pressure region in the core of the vortex. For higher cavitation numbers this vortex also causes a corkscrew type of flow through the injection hole which is likely to be responsible for the hollow cone fuel sprays of VCO nozzles reported in [18, 19]. The helical distortion of the cavitation structures could be confirmed with the high-speed imaging (lower rows in Figure 11 and Figure 12; Figure 19). This phenomenon is more apparent at lower needle lift (see also Figure 19).

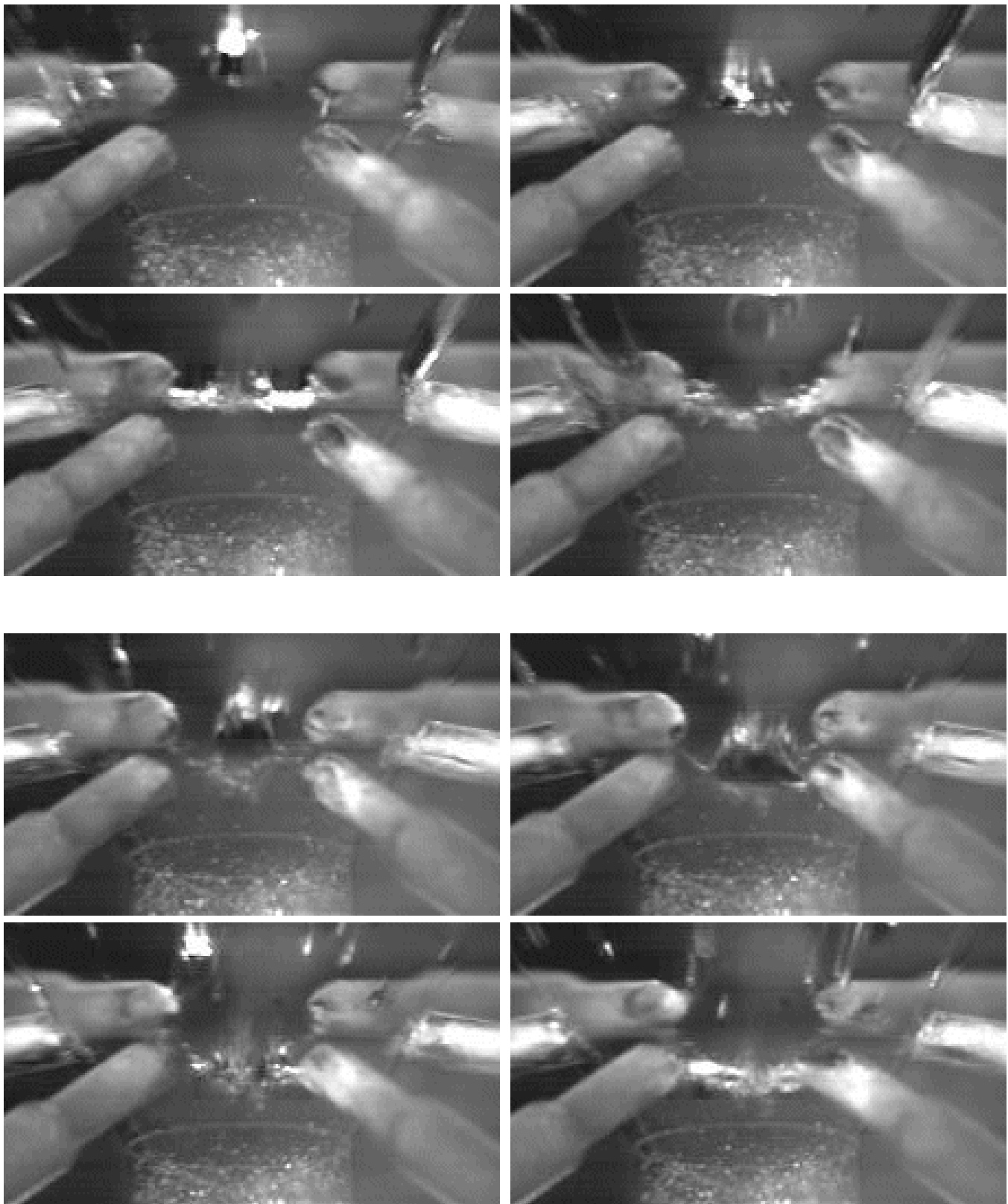


Figure 10: Two image sequences (each left to right and top to bottom) showing an air bubble getting sucked into the low pressure region of a vortex present in the volume between needle and needle seat of the VCO type nozzle. The large bubble disintegrates into a cloud of small bubbles which then fill the vortex core to form a bubble string (not cavitation yet!). A schematic of the imaging area is given in Figure 8. Note, that the small bubbles in the tip volume do not show any appreciable movement which indicates stagnant flow there.

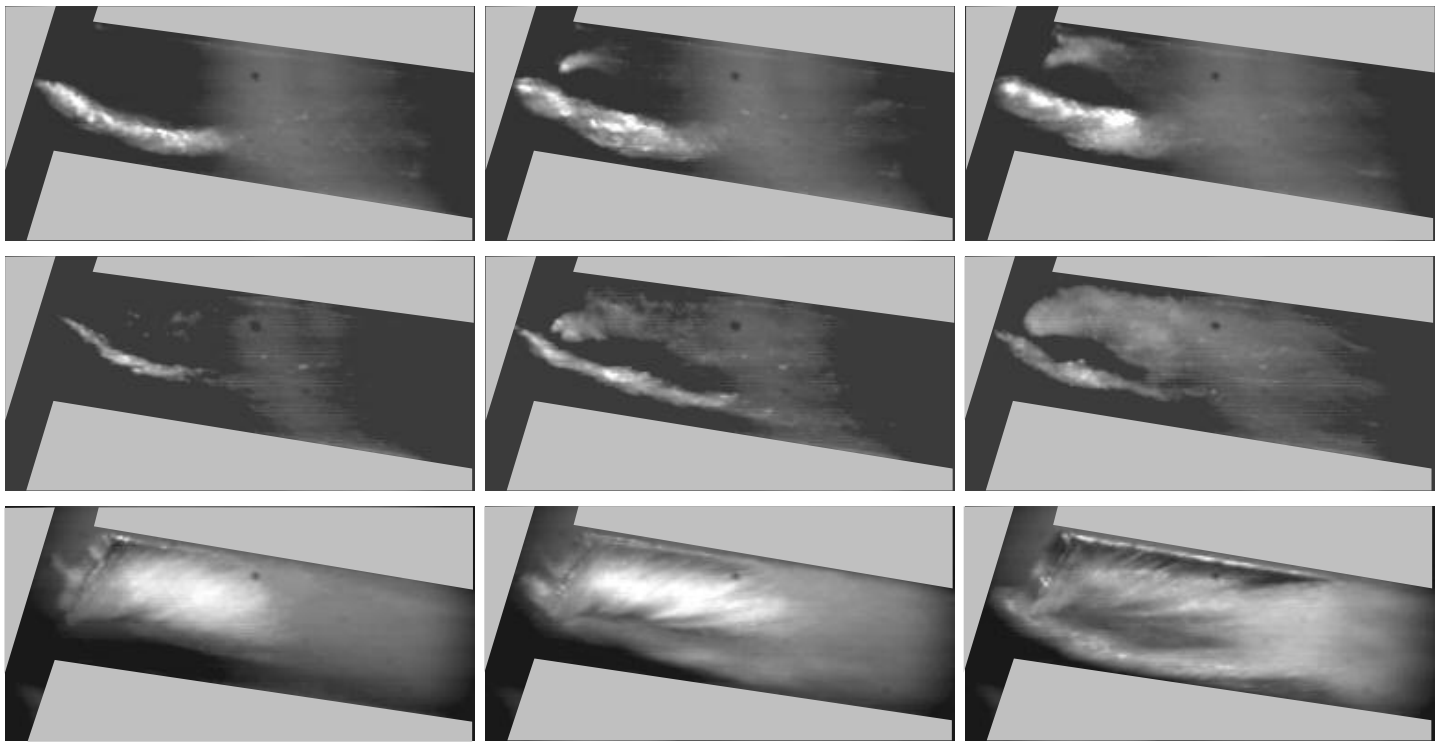


Figure 11: High-speed video images of steady-state cavitating flow through one hole of the VCO type nozzle with needle lift = 1.6mm and CN = 0.81 (upper row), CN = 1.02 (middle row), CN = 1.52 (bottom row); The images of one row are from the same video sequence, but they are not directly consecutive. For all conditions the ‘needle string’ is visible which is created by the vortex flow around the injection hole axis. This vortex extends out of the hole onto the needle surface. For the lower CN ‘corner cavitation’ is also apparent (see further below and Figure 17). In the bottom row the film flow structure shows a corkscrew pattern due to the vortex in the hole.

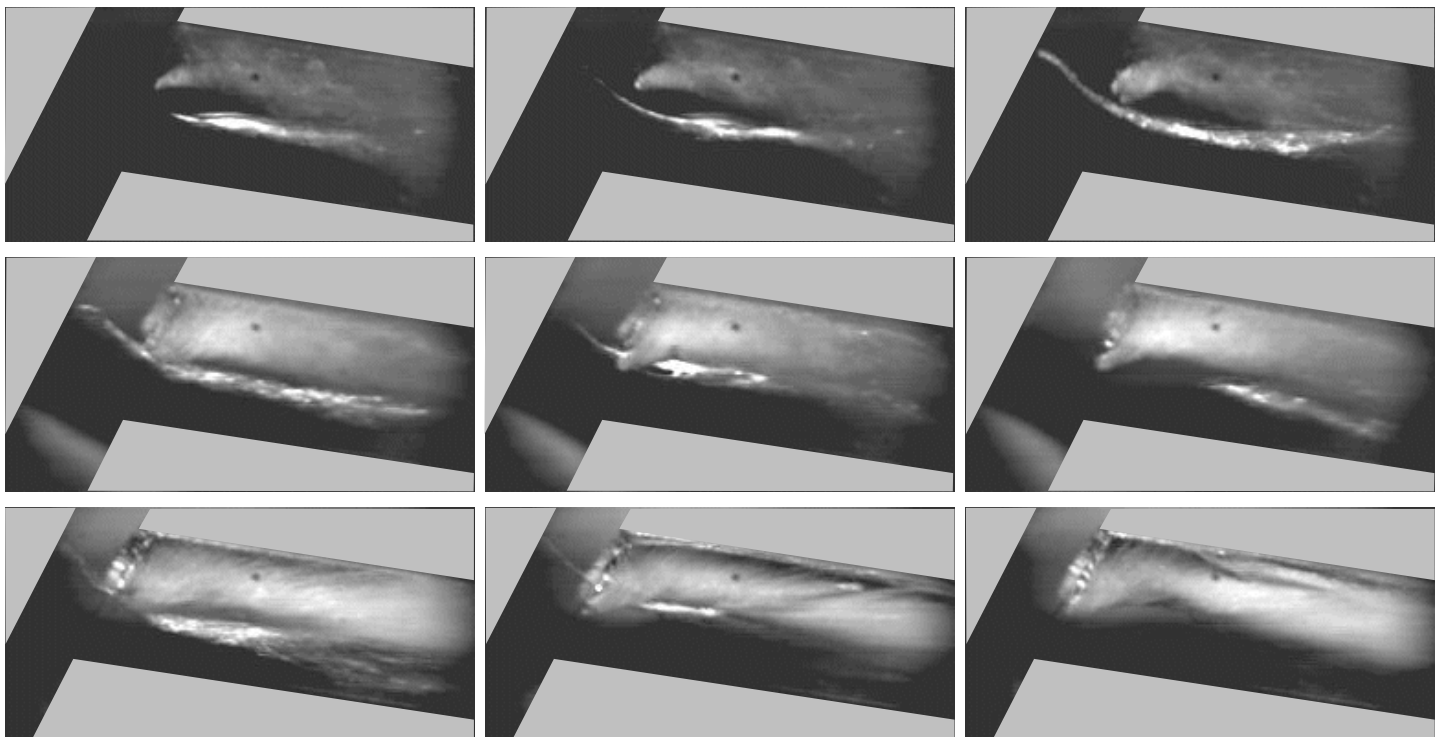


Figure 12: High-speed video images of steady-state cavitating flow through one hole of the VCO type nozzle with needle lift = 4.0mm and CN = 0.71 (upper row), CN = 0.94 (middle row), CN = 1.58 (bottom row); The images of one row are from the same video sequence, but they are not directly consecutive. The ‘needle string’ and its dynamic behaviour are apparent. Mostly the strings are attached to the needle surface, but frequently they detach and move downstream before they reattach without being totally conveyed out of the hole. In the upper row the ‘corner cavitation’ develops (see further below and Figure 17) and in the middle row it can be seen how the ‘corner cavitation’ spreads along the upper hole inlet edge. In the bottom row the film flow structure shows a corkscrew pattern.

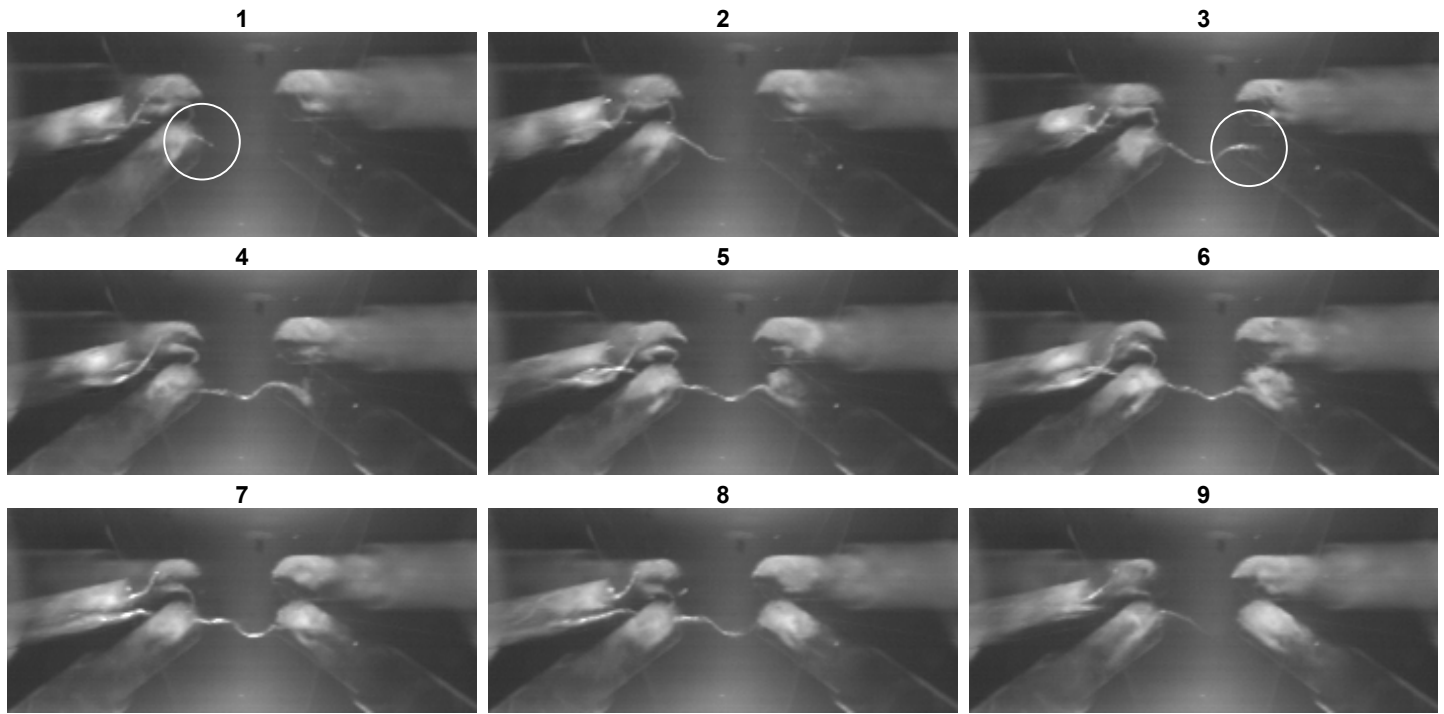


Figure 13: String induced cavitation in the mini-sac type nozzle with needle lift = 1.6mm and CN = 2.39; The images are shown successively from left to right and top to bottom with time gaps of approximately 0.2ms. The existing vortex flow with low pressure core between the two holes closest to the viewer sucks existing cavitation bubbles out of the left hole (1) and a string starts to form. The string structure extends along the vortex's core (2) until it reaches the right hole inlet (3). There the string diffuses into a bubble cone (4) and bubbles get immediately sucked into the recirculation zone of the hole inlet (5). Hole cavitation initiates and develops further (6-9), since the bubbles serve as cavitation nuclei. The string itself disappears after the hole cavitation has developed (9).

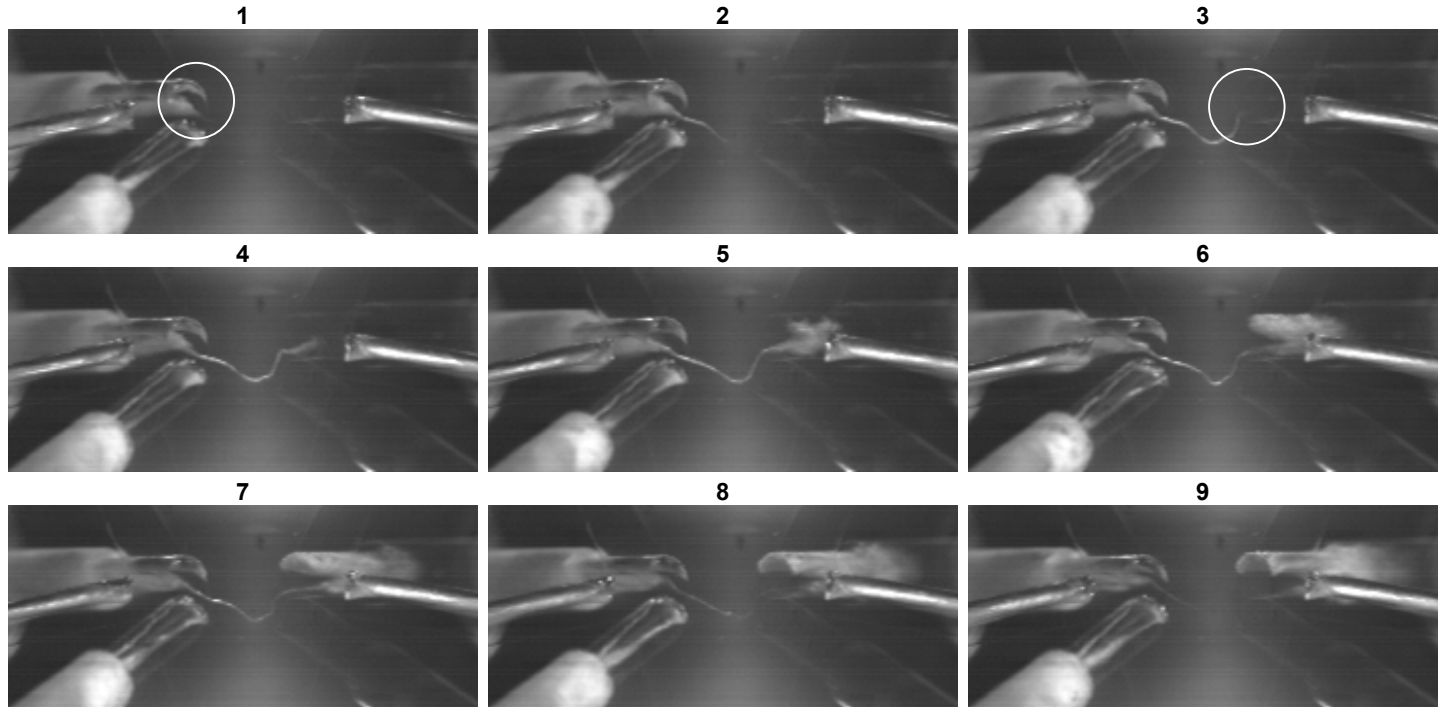


Figure 14: String induced cavitation in the mini-sac type nozzle with needle lift = 6.0mm and CN = 4.57; The images are shown successively from left to right and top to bottom with time gaps of approximately 0.2ms; The existing vortex flow with low pressure core between the two holes furthest from the viewer sucks existing cavitation bubbles out of the left hole (1) and a string starts to form. The string structure extends along the vortex's core (2) until it reaches the right hole inlet (3). There the string diffuses into a bubble cone (4) and bubbles get immediately sucked into the recirculation zone of the hole inlet (5). Hole cavitation initiates and develops further (6-9), since the bubbles serve as cavitation nuclei. The string itself disappears after the hole cavitation has developed (9).

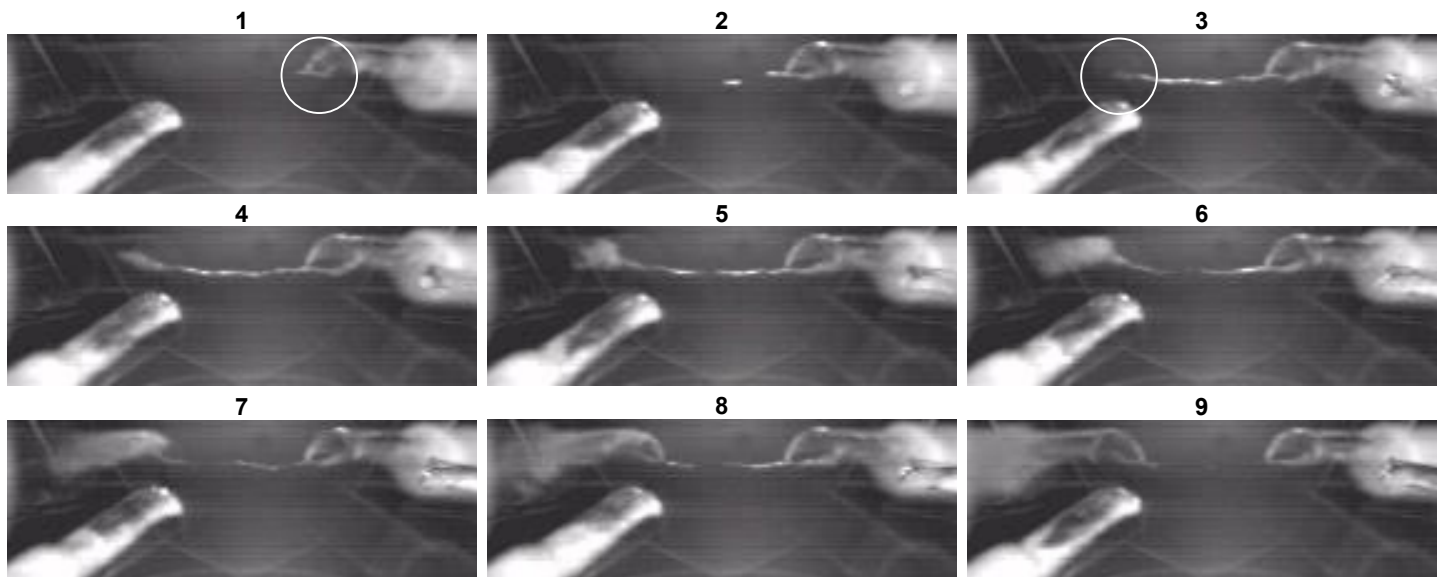


Figure 15: String induced cavitation in the VCO type nozzle with needle lift = 6.0mm and CN = 4.34; The images are shown successively from left to right and top to bottom with time gaps of approximately 0.2ms; The two holes furthest away from the viewer are involved in the process which can be described as in Figure 13 and Figure 14.

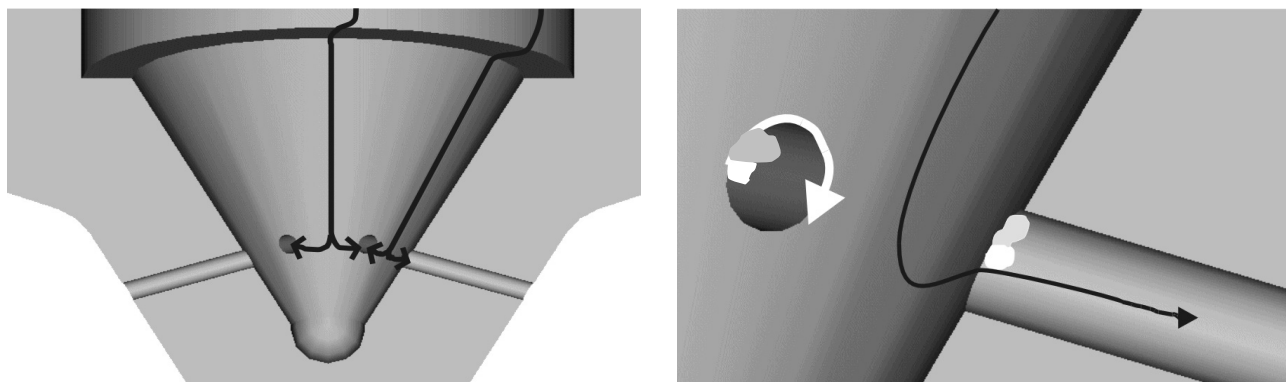


Figure 16: Schematic streaklines of the fluid flow entering the injection holes from the side (left). The flow around the side corners of the injection holes creates recirculation zones and low pressure regions there. This is where the 'corner cavitation' initiates (white areas in the right picture). Once the cavitation incerts, it starts to spread along the upper edge of the hole inlet (see white arrow and grey areas) and finally occupies the upper part of the inlet edge which leads to fully developed hole cavitation (cp. Figure 17).

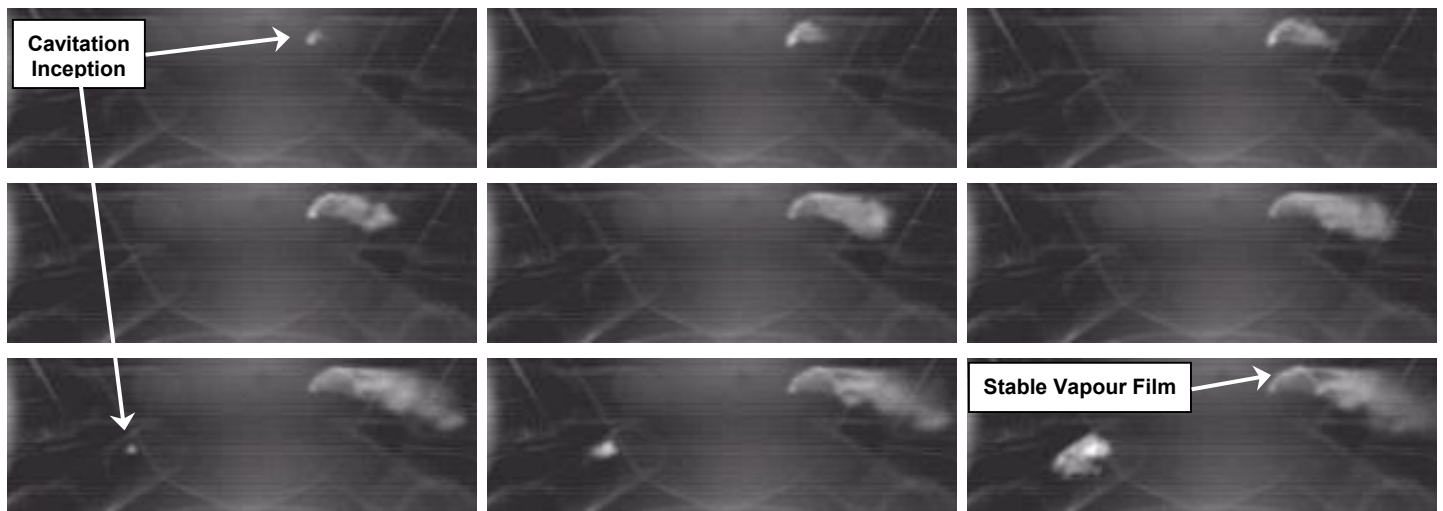


Figure 17: Cavitation initiates at one side of the injection hole inlet in the VCO type nozzle with needle lift = 6.0mm and CN = 4.34; The images are shown successively from left to right and top to bottom with time gaps of approximately 0.2ms. Cavitation arches along the upper hole inlet edge until film cavitation is fully developed.

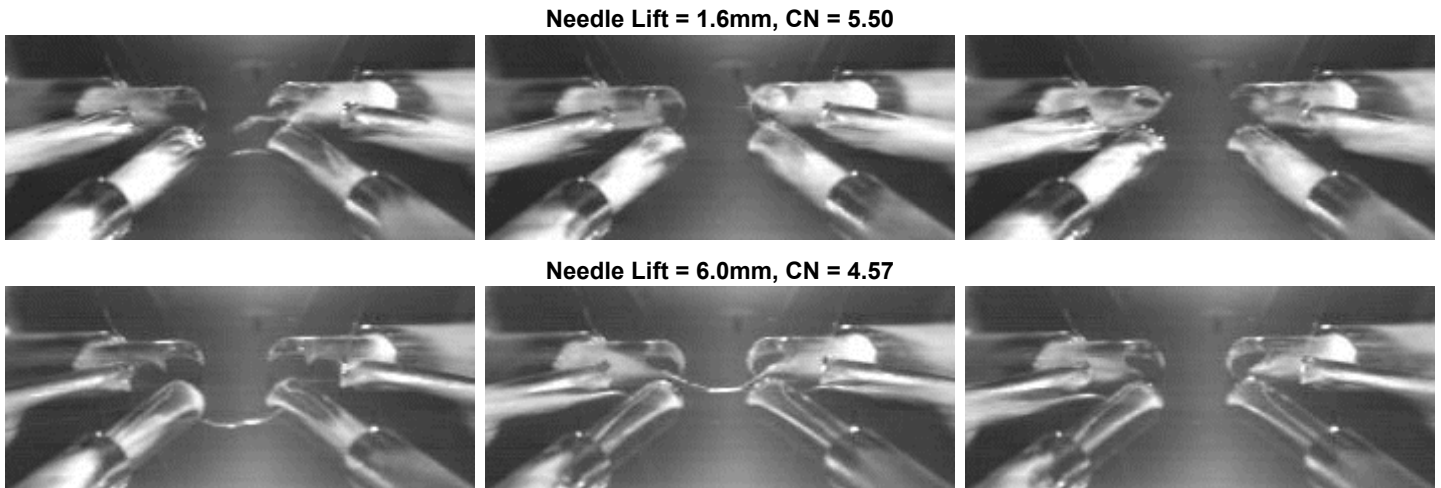


Figure 18: Fully developed flow through the mini-sac type nozzle showing film and string cavitation. Both rows show independent pictures of the given flow conditions. For the lower needle lift it is apparent that the flow structures are more transient than for the higher needle lift. Especially the strings are more frequent and the cavitation film is more stable and extends to the hole exit for high lift, despite the fact that the cavitation number is slightly less than for the low lift condition.

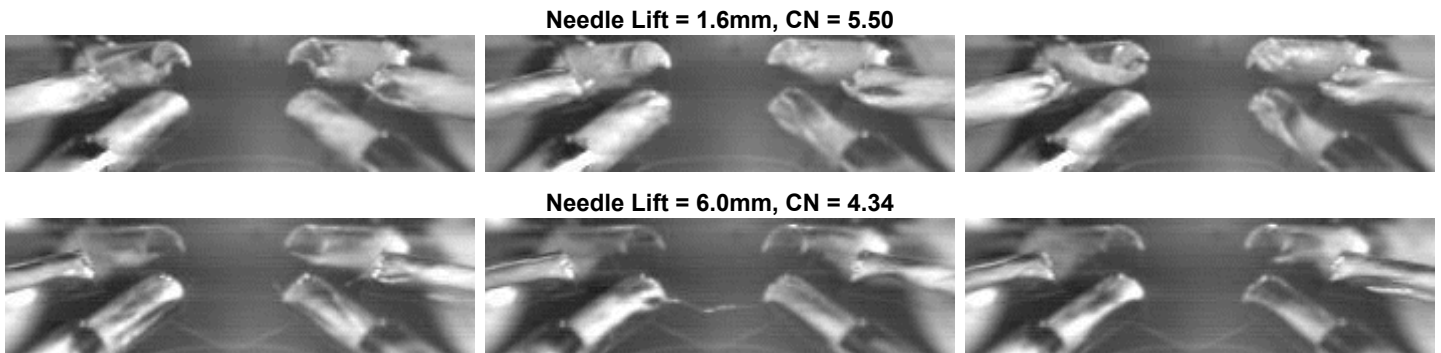


Figure 19: Fully developed flow through the VCO type nozzle showing film and string cavitation. Both rows show independent pictures of the given flow conditions. Again, for the lower needle lift it is apparent that the flow structures are more transient than for the higher needle lift. In the upper row it can be seen that only the 'needle strings' occur and that there is an obvious spiral movement of the cavitation structures inside the hole (cp. Figure 11). For higher needle lift the cavitation film becomes more stable and the 'needle strings' less frequent, but 'hole connecting strings' start to appear.

Cavitation Inception

It is interesting to investigate the moment the injection starts, when the highly transient flow through the nozzle develops. With the enlarged injector it is not possible to simulate the fast opening of the needle which occurs in a real-size production injector at start of injection. Therefore, the needle in the model nozzles was set to fixed positions and the flow rate was increased rapidly by operating the pumps in order to simulate the transient flow conditions present at the start of injection. During this acceleration phase of the liquid through the model nozzles, the high-speed video camera was able to capture the cavitation inception.

In all cases investigated, the transition from non-cavitating to cavitating hole flow did not occur simultaneously for all injection holes, but randomly hole by hole with short delays. This revealed again that the nozzle flow develops transiently and that the holes are "throttled" intermittently due to the hole-to-hole variations of

the recirculation zones, even for a symmetric nozzle geometry. After the first hole starts to cavitate, the cavitation pattern undergoes the development described above and in [20]. With increasing flow rate the other holes begin to cavitate successively in a random manner. The transition through all cavitation patterns happens there with increasing speed due to the accelerating flow. Up to now it was not really clear which flow phenomena influence the cavitation inception of the single holes besides the increasing flow rate and, consequently, increasing pressure drop around the upper corner of the hole inlet. With the high-speed video image sequences it could be seen that the flow entering the injection hole from the side, as well as the cavitation strings, play a major role in further cavitation inception. In Figure 13 through Figure 15 the string induced hole cavitation is shown in representative sequences of pictures which were taken approximately every 0.2ms. The formation of the cavitation induced by strings can be described as follows: When the flow rate through the nozzle picks up after the pumps are operated and the vortex

flow in the volume between two adjacent holes is strong enough to create the necessary low pressure in its core region, nuclei for the string cavitation, in form of already existing vapour bubbles, are sucked out of the cavitating zone of one of the holes into the vortex's core. There the bubbles begin to form the continuous vapour string which extends rapidly along the vortex's low pressure region into a neighbouring injection hole. Once the string enters this hole, it disintegrates into bubbles again (cp. Figure 9) due to the much lower pressure in the recirculation zone of the hole inlet area and the significantly increasing flow velocity when the fluid, together with the string, enters the hole (cp. velocity plots in Figure 23 and Figure 24). The bubbles, originating from the diffused string, get immediately sucked into the low pressure core of the recirculation zone in the upper part of the hole inlet. This leads to a disturbance of the meta-stable liquid in that area, apparently like heterogeneous nucleation, and the fluid ruptures, i.e. hole cavitation sets in. Almost immediately after the recirculation zone is filled with cavitation bubbles the fluid flow around the upper hole inlet corner separates from the upper hole surface which leads to pre-film, or fully developed vapour film cavitation, depending on the cavitation number, i.e. flow conditions. All three stages of the hole cavitation development (see further above) are passed almost instantaneously. Due to the transient nature of the sac vortex flow, the cavitation string disappears shortly after the induction of the hole cavitation.

In addition to the cavitation strings, another important factor of cavitation inception is the liquid entering the hole laterally when the flow rate picks up. Since all the upstream fluid, coming from the annulus regions between the hole planes needs, to exit the nozzle through the holes and due to the increased momentum of that flow, it takes a little longer for the liquid to turn into the hole. Therefore, a substantial part of the flow cannot enter the hole around the top corner but has to move from the volume between the injection holes into the holes around their side corners (Figure 16). Because of the transient conditions inside the nozzle, this flow from the side can create recirculation zones at both sides of the hole which causes the pressure of the liquid to drop low enough within this recirculation areas, so that cavitation can be initiated at the side corners of the hole inlet (namely 'corner cavitation') before cavitation starts at the top corner. After the onset at one corner, cavitation rapidly spreads along the upper part of the hole inlet edge and a stable vapour film develops. This process is shown with a representative image sequence in Figure 17.

Developed Cavitation

In general, for steady-state model nozzle flow the transitions from bubbly flow through pre-film to film stage cavitation, which were observed in the CCD still images [15, 20], could be identified in the high-speed videos as well as the cavitation number was increased accordingly. For all investigated cavitation numbers it seems, that with low needle lift the cavitation structures are more unsta-

ble due to the increased flow turbulence caused by the bottle neck effect in the needle seat region (cp. LDV results further below). Especially the vapour film in case of higher cavitation numbers exhibits a highly transient behaviour. Cycles of separation and reattachment of the cavitation film structures could be observed. This is apparent in Figure 18 and Figure 19 as the cavitation pattern at the upper side of the injection hole changes colour between shiny dark (fully developed film) and cloudy white (attached bubbly pre-film). When the needle lift is increased, the film becomes more stable and reaches the hole exit under higher cavitation number conditions. The development of both string type cavitation patterns also strongly depends on the needle lift, since a larger nozzle tip volume, i.e. higher needle lift, enhances the necessary vortex formation. In case of low needle lift there was no appreciable formation of 'hole connecting strings' in the VCO nozzle, only the 'needle strings' were frequently apparent. With increasing needle lift, transient strings connecting two adjacent holes could be observed and the 'needle strings' became less frequent. Within the sac volume of the mini-sac nozzle it could be seen for low needle lift, that unstable strings formed and that they became more stable and frequent with increasing lift (Figure 18).

In order to gain visual information about the dynamic behaviour of the flow in the lower nozzle sac volume, where no cavitation structures occurred, the upstream flow was seeded with air bubbles. The bubbles followed the flow with no appreciable delay and it could be seen that the cross flow occurs close to the needle tip and that there is almost no liquid movement through the tip volume for both nozzle types. Therefore, no influence on the cavitating hole flow is expected to come from this region. This was also confirmed by the LDV measurements.

LDV MEASUREMENTS

Nozzle Flow Field

Figure 20 illustrates the velocity profiles obtained for the non-cavitating flow condition highlighted in Table 1. In Figure 21 the velocity profiles obtained in the injection hole for the same flow condition are depicted. All velocity vectors were assembled from the measured horizontal and vertical velocity components for each measurement location within the conical mini-sac type nozzle.

As can be seen in Figure 20, the flow in the annulus and in the injection hole inlet vicinity is very symmetric around the vertical axis of the nozzle. Only further down in the sac volume it is apparent that the rather low flow velocities do not have a preferred direction anymore. Most of the cross flow through the sac volume occurs just around the needle tip and therefore the flow field in the bottom part of the sac is almost stagnant (see also Figure 10).

When the liquid turns from the annulus into the injection hole, the flow velocities increase rapidly due to the de-

crease of cross sectional flow area as can be seen in Figure 20 and Figure 21. The highest velocities occur at the upper corner of the hole inlet where also the lowest fluid pressures can be expected (cp. [4, 9, 11]).

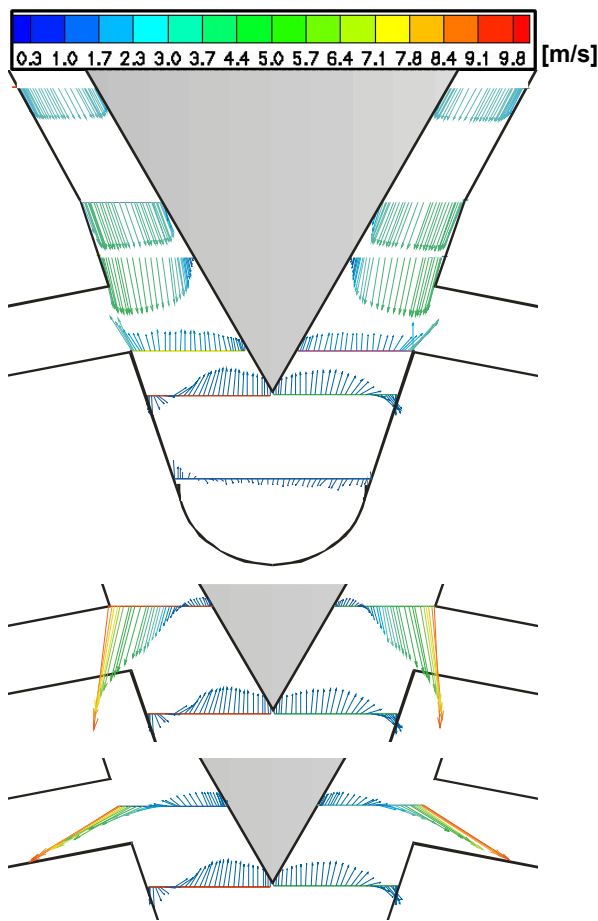


Figure 20: Representative velocity profiles in annulus and sac volume of the mini-sac type nozzle for needle lift = 6.0mm and CN = 0.45; Measurement locations see Figure 7

This pressure drop around the corner leads to a recirculation zone which stretches downstream over a length of about one third of the injection hole length and occupies there roughly the upper third of the hole diameter. Further downstream the recirculation zone disappears and the velocity profile is more likely to be distributed over the hole diameter as in a developed pipe flow.

Since string cavitation is always occurring for higher cavitation numbers and the vortices, which lead to the strings, are present even for non-cavitating flow conditions [20], it was of interest to investigate the influence of these flow patterns on the flow turbulence levels in the injection hole inlet vicinity. Therefore, LDV measurements according to the conditions of Table 1 were carried out at the locations given in Figure 22.

Figure 23 and Figure 24 show the normalised profiles for the local mean velocities, V (depicted with triangles), and the turbulent kinetic energy, TKE (depicted with squares), at $x = 6.2\text{mm}$ and $x = 8.5\text{mm}$, respectively. The increase of the plot symbol size corresponds to in-

creasing cavitation numbers. On the abscissa the measured values for the mean velocity, normalised with the bulk injection velocity, U_{inj} , are plotted versus the normalised vertical measurement positions on the ordinate. The TKE values, as proportional to RMS^2 , are normalised with the maximum value of the turbulent kinetic energy ($\sim \text{RMS}_{\text{max}}^2$) for both measurement planes. Like V , the normalised TKE values are plotted versus the normalised position of the measurement location.

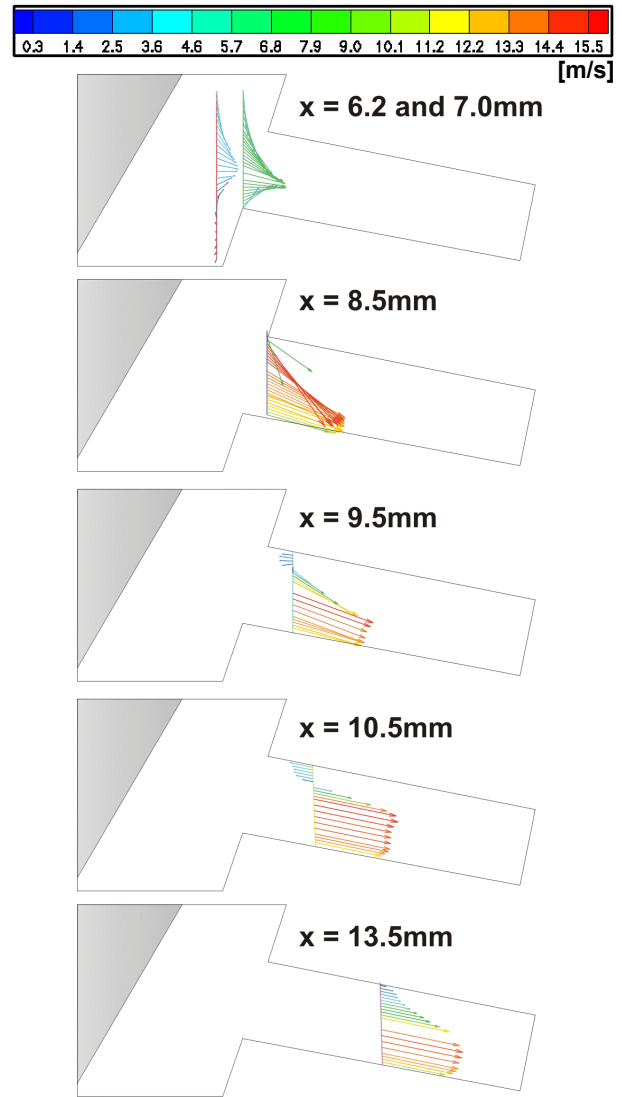


Figure 21: Representative velocity profiles in one injection hole of the mini-sac type nozzle for needle lift = 6.0mm and CN = 0.45; Measurement locations see Figure 6

From Figure 23 it is apparent that despite the varying flow conditions there is no appreciable change in the velocity and TKE at this location in front of the injection hole. The turbulence levels have peaks where the largest velocity gradient is present, which is expected, but no influence from the cavitation structures can be detected. It seems that the vortices create only a very weak turbulence field that immediately dissipates and diffuses into the surrounding bulk flow which also enters the hole. At the location where cavitation strings occur it was not possible to obtain sufficient LDV signals for CN

$= 0.83$. Therefore, the plots for the velocity and TKE are not continuous between $z = 11.8\text{mm}$ and $z = 14.2\text{mm}$ at this flow condition.

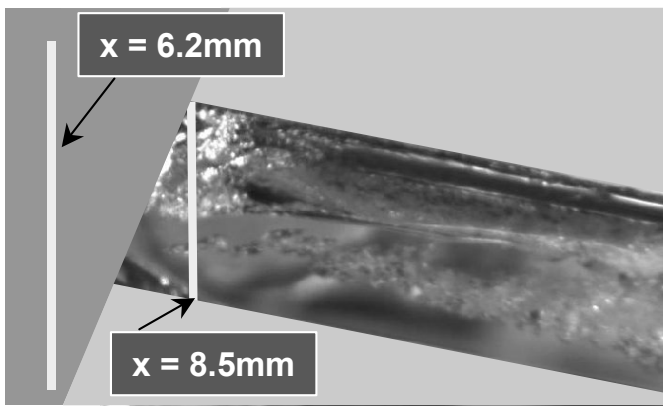


Figure 22: Hole inlet measurement locations inside one injection hole of the mini-sac type nozzle (cp. Figure 6)

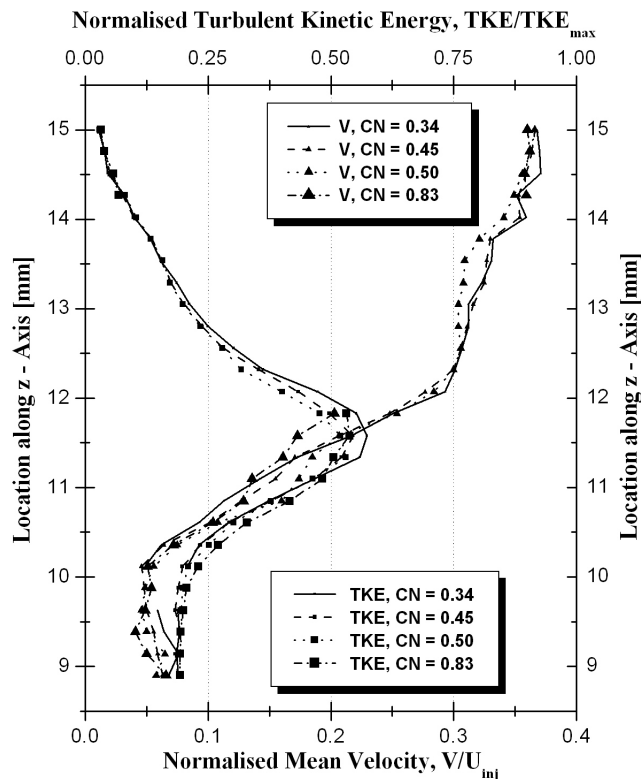


Figure 23: Needle lift = 6.0mm, $\text{Re} = 21000$, $x = 6.2\text{mm}$

Different information is provided by Figure 24, where the measurements were taken right in the hole inlet. Due to the optically dense cavitating recirculation zone and the resulting pre-film cavitation structure it was not possible to obtain LDV results in the upper half of the hole for $\text{CN} = 0.50$ and $\text{CN} = 0.83$. Even though, it is now very clear that with increasing cavitation number not only the TKE, but also the local mean velocities within the bulk flow through the lower half of the hole inlet are influenced by cavitation. Due to the enforced cavitation conditions the recirculation zone is more or less replaced by the pre-

film stage cavitation which restricts the hole flow less than the recirculation zone.

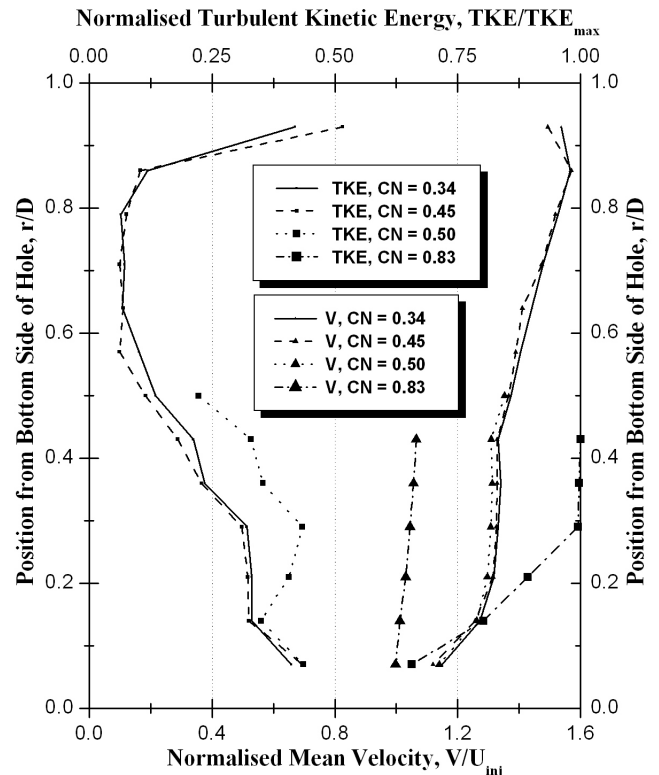


Figure 24: Needle lift = 6.0mm, $\text{Re} = 21000$, $x = 8.5\text{mm}$

As a result, the velocity of the fluid flow through the lower half of the hole is reduced with increasing cavitation number but no change in flow rate. The turbulence created by the hole inlet cavitation and the entering strings is now not diffused and an apparent increase of the TKE with increasing cavitation number can be seen. Compared with the results shown in Figure 23, the flow velocities right at the hole inlet are, as expected, higher than in front of the inlet area.

Velocity Profiles in Injection Holes

Extended measurements within the injection hole were taken for all non-cavitating and cavitating flow conditions given in Table 1. Figure 25 shows the measurement locations in one of the injection holes for this first series of hole measurements. Figure 27 and Figure 28 depict representative profiles for the local mean velocity (depicted with triangles) and the RMS values (depicted with squares) at these locations. The increase of the plot symbol size corresponds again to increasing cavitation numbers. On the abscissa the measured values for the mean velocity and the RMS values are normalised with the bulk injection velocity, U_{inj} , and they are plotted versus the dimensionless vertical positions of the measurement location within the hole (r/D from bottom side of the hole) on the ordinate. The same nomenclature is also valid for the graphs showing representative results of the second series of LDV measurements within the injection hole (Figure 29 and Figure 30).

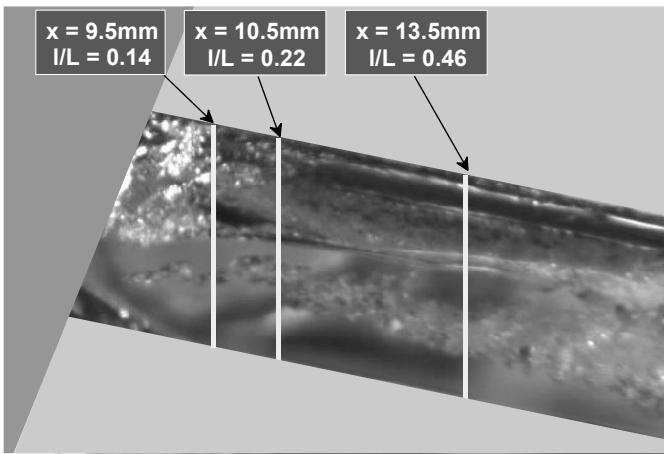


Figure 25: Locations inside one injection hole for the first series of LDV measurements

For the first series of measurements only the cavitation number (pressure level of injection) was changed, but the Reynolds number (flow rate) was kept constant per needle lift setting according to Table 1. For the second series of measurements it was possible to extend the LDV investigations further towards the hole exit with the additional location of $x = 16.5\text{mm}$ (Figure 26). Additionally, an increase of the cavitation and Reynolds number was realised, which enabled the investigation of higher flow rates and enhanced cavitation conditions.

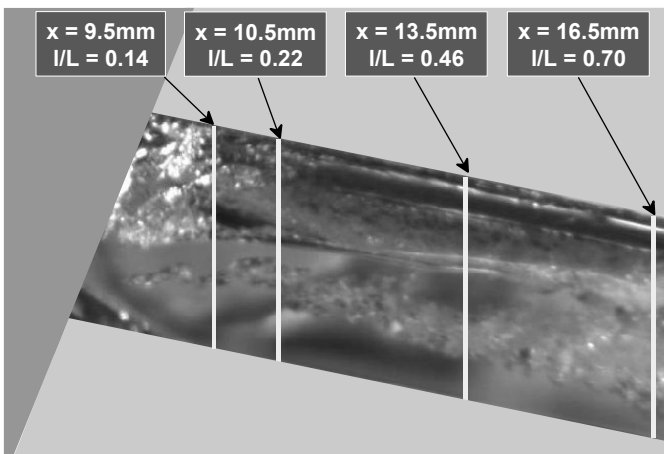


Figure 26: Locations inside one injection hole for the second series of LDV measurements

A first observation from the plots of the local velocity at $x = 9.5\text{mm}$ in Figure 27 and Figure 28 confirms the earlier finding that the recirculation zone close to the hole inlet is reduced with increasing cavitation number. This is apparent in the upward movement of the zero-crossings of the velocity plots (“eye” of the recirculation zone) for higher cavitation numbers. Since the flow through the injection hole is less restricted at the hole inlet when the recirculation zone is flattened, the liquid has more area to flow through and therefore the bulk velocity below the recirculation zone ($r/D < 0.7$) is decreased for increased cavitation, but constant Reynolds number. This trend is still visible further downstream ($x = 10.5\text{mm}$ and $x =$

13.5mm) for both needle settings. The recirculation zone is also reduced with increasing needle lift. That can be seen for both series of measurements. When looking at the RMS levels within the lower half of the hole flow ($r/D < 0.5$) it becomes apparent that for $x = 9.5\text{mm}$ there is an increase with increasing cavitation number. This indicates that here the occurring cavitation structures enhance the turbulence under the given conditions even for the slightly decreased flow velocities. Note that this effect is stronger for the higher needle lift.

At the position $x = 13.5\text{mm}$ one sees that the RMS levels are almost the same for the different cavitation numbers per needle lift setting. In connection with the theory of turbulent bubble break-up [21, 22] it is believed that the “additional”, cavitation induced, turbulence, coming from the hole inlet region, is mostly consumed by the bubble break-up process which takes place along the hole length. That assumption is backed up by the results from the second series of LDV measurements (cp. Figure 31 and Figure 32). In addition, violent bubble collapse processes, which are considered to increase flow turbulence, are not likely to occur due to the short residence time of the bubbles inside the hole under the given flow conditions [2, 23, 24]. Looking at all six graphs of Figure 27 and Figure 28, one recognises that the RMS levels for the low needle position are to some extent higher as those for higher needle lift. This can also be observed in Figure 29 and Figure 30. The reason for that trend is the increased bottle neck effect at the needle seat of the mini-sac nozzle in case of low needle lift. Due to the reduced flow passage the liquid needs to squeeze through a smaller flow area and is therefore locally accelerated which slightly increases the turbulence levels from this point onwards.

In addition to the velocities and the RMS values, it is interesting to obtain the TKE distribution within the injection hole. For this, the turbulent kinetic energy was obtained from the RMS values at each measurement point as done above. In each vertical measurement plane these values were then averaged for the liquid bulk flow region, i.e. only points up to roughly half the hole diameter from the bottom side of the hole were considered. These averages were then normalised with the maximum average value from all flow and needle lift conditions. As can be seen in Figure 31 and Figure 32, the liquid flow has increased turbulent kinetic energy with increasing cavitation number. At the same time as the liquid, under various cavitation conditions, moves downstream, its turbulence levels approach asymptotically the level of the non-cavitating flow ($CN = 44$ for needle lift = 1.6mm and $CN = 0.45$ for needle lift = 6.0mm). This supports the hypotheses that the occurring break-up of the cavitation structures is driven by the turbulent kinetic energy and therefore reduces the turbulence levels in the liquid while it is travelling through the hole. Overall, the turbulent kinetic energy levels are higher in case of the low needle lift setting compared to the higher lift condition due to the already mentioned bottle neck effect in the needle seat region.

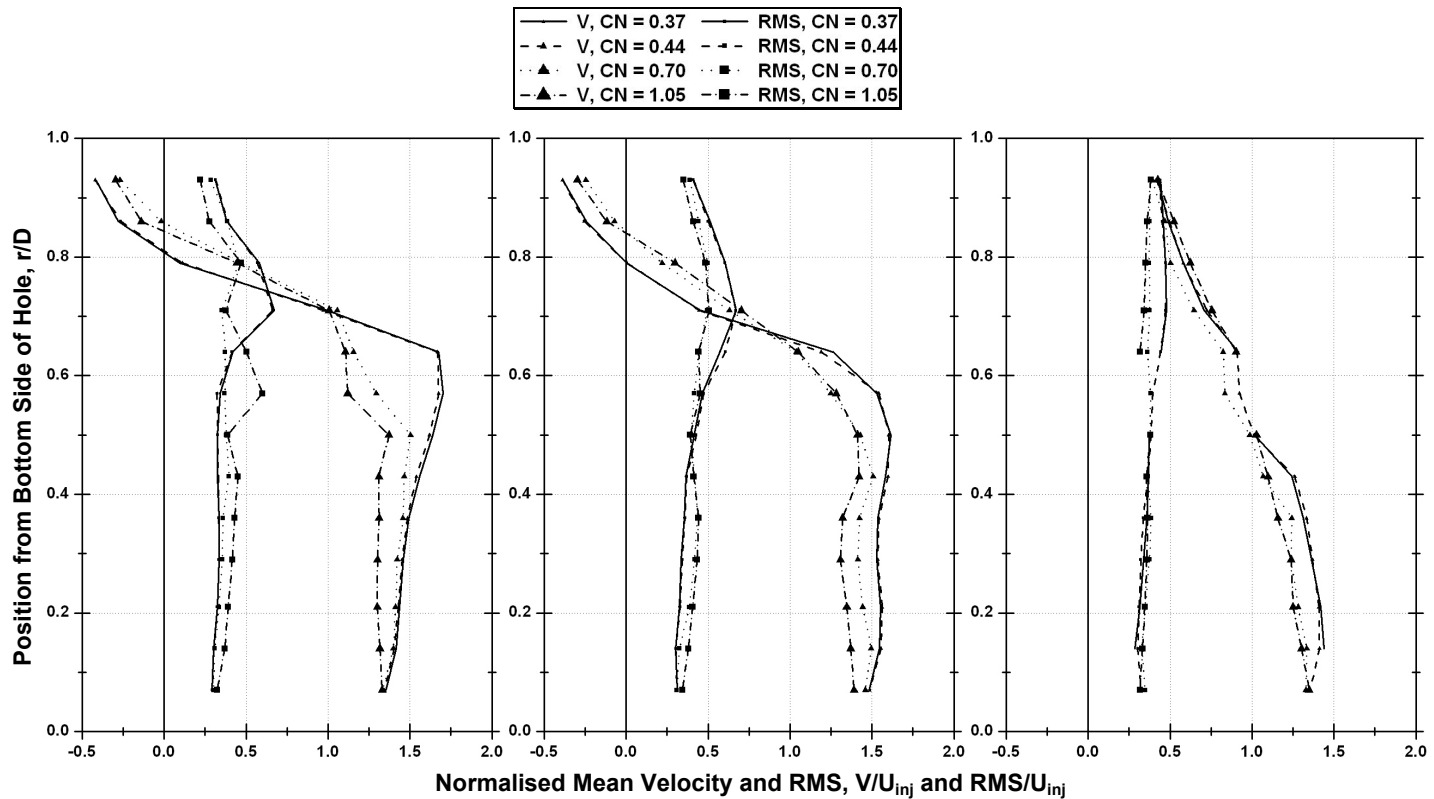


Figure 27: Results from first series of LDV measurements; Needle lift = 1.6mm, $Re = 18000$, $x = 9.5\text{mm}$ (left), $x = 10.5\text{mm}$ (middle) and $x = 13.5\text{mm}$ (right)

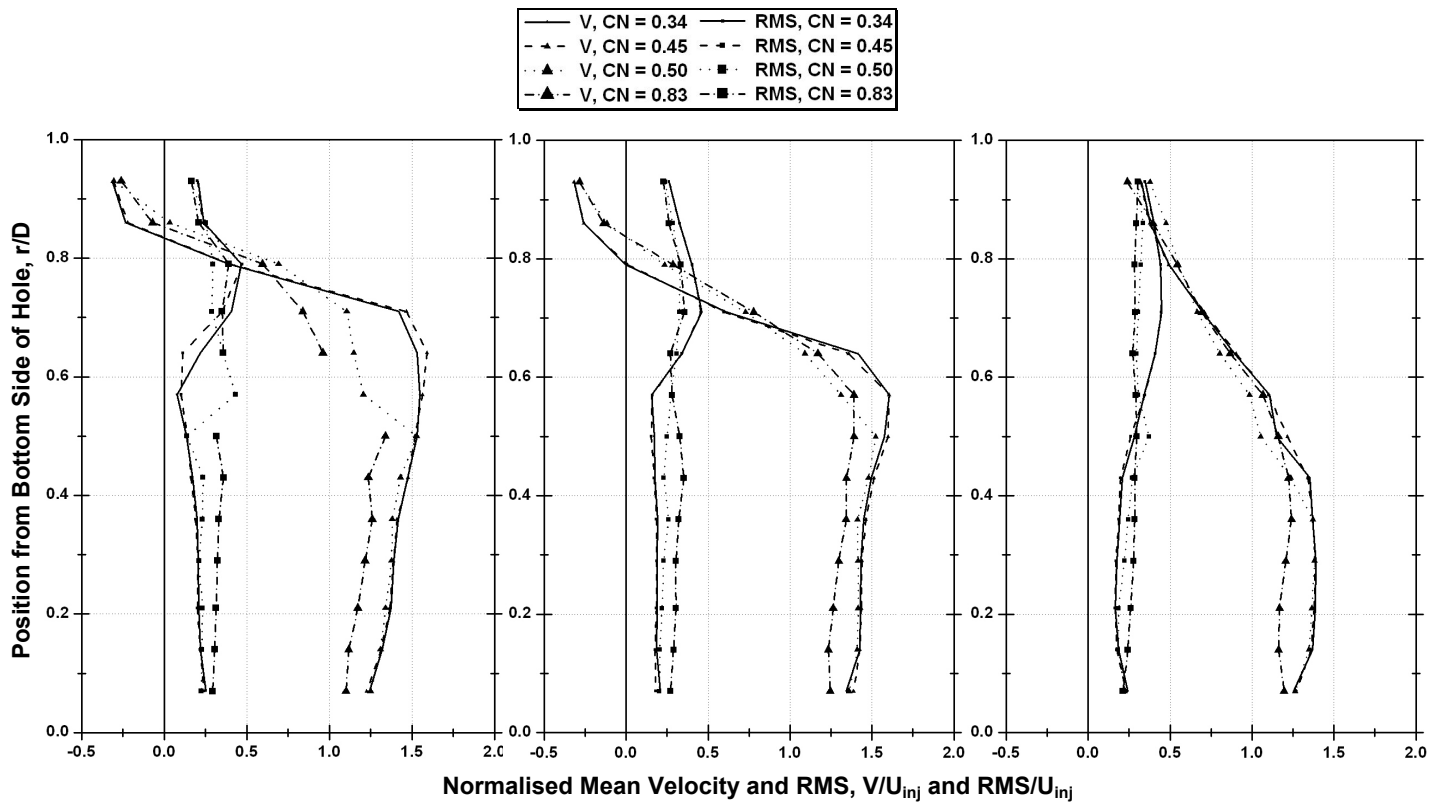
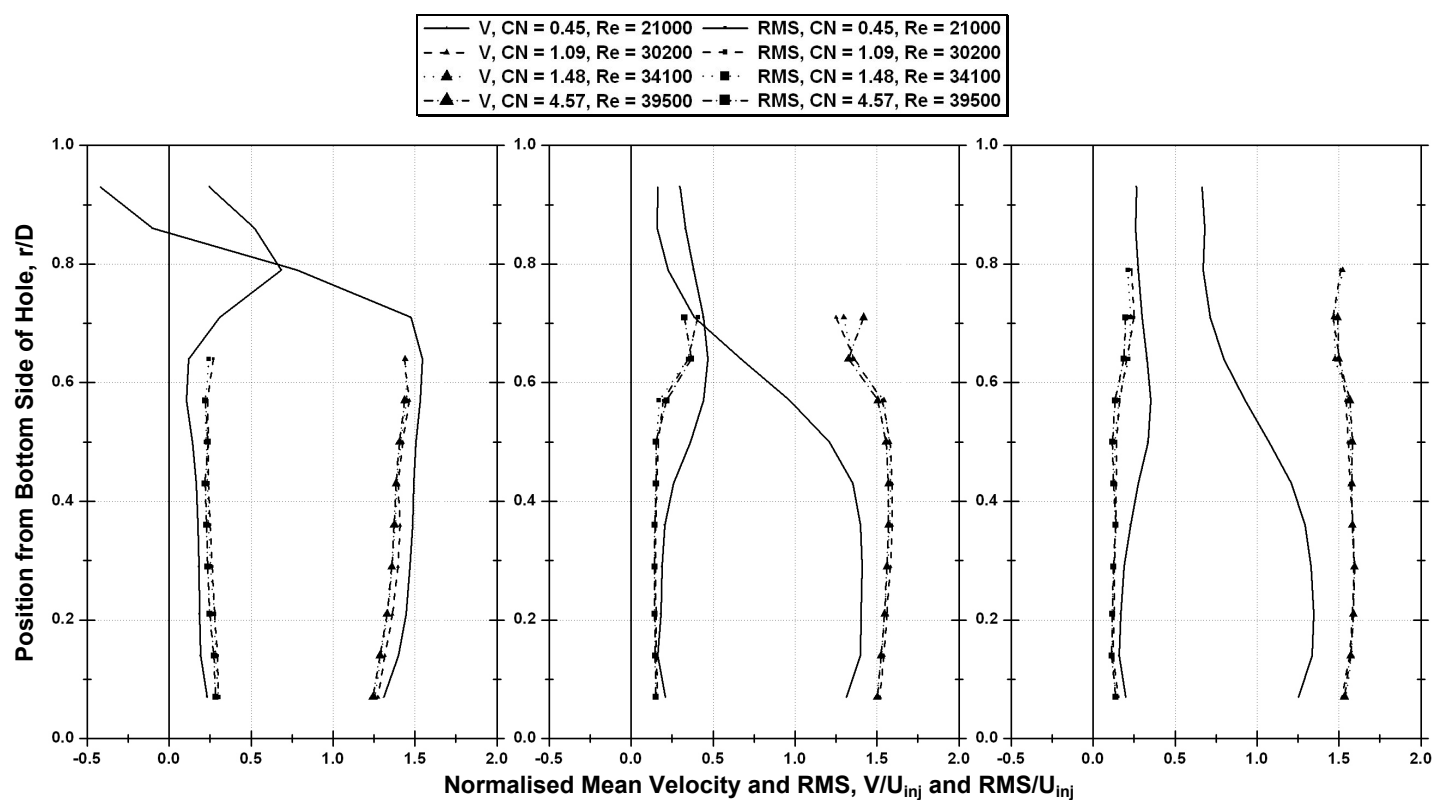
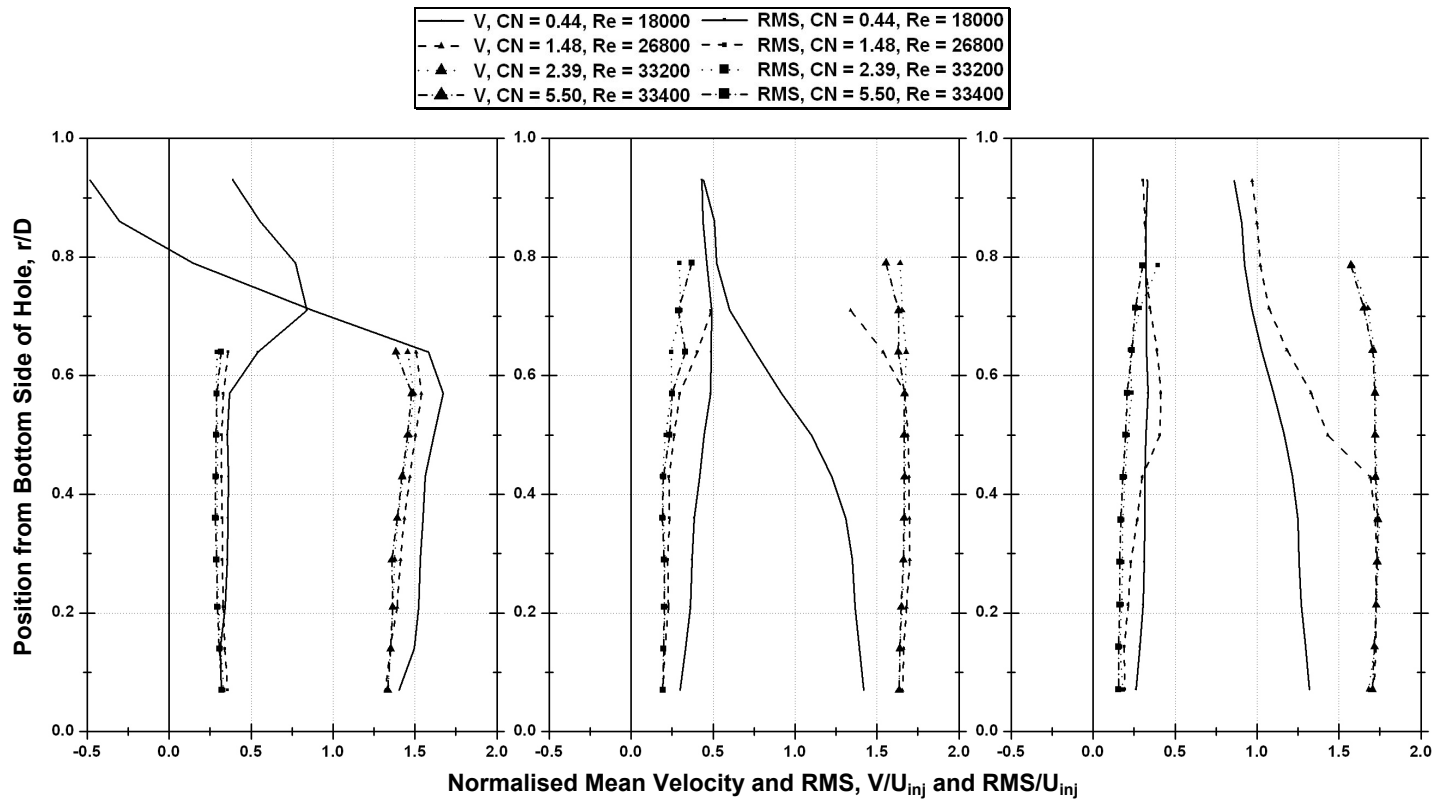


Figure 28: Results from first series of LDV measurements; Needle lift = 6.0mm, $Re = 21000$, $x = 9.5\text{mm}$ (left), $x = 10.5\text{mm}$ (middle) and $x = 13.5\text{mm}$ (right)



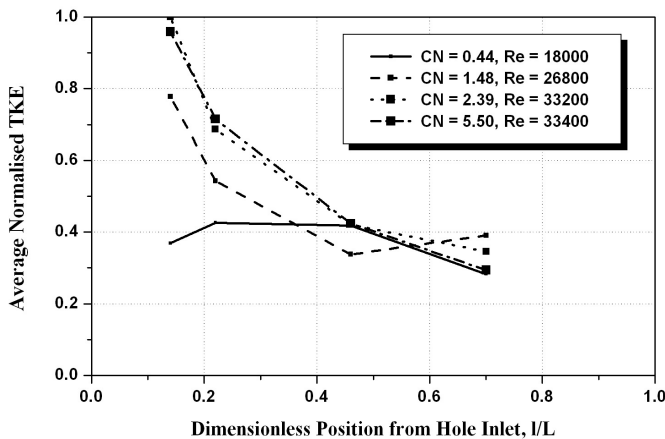


Figure 31: Normalised turbulent kinetic energy in the liquid flow under conditions of the second series of LDV measurements; Needle lift = 1.6mm

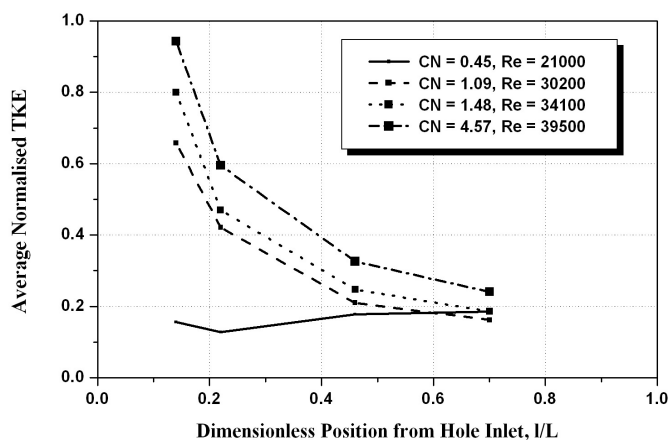


Figure 32: Normalised turbulent kinetic energy in the liquid flow under conditions of the second series of LDV measurements; Needle lift = 6.0mm

CONCLUSIONS

The dynamic behaviour of incipient and developed cavitation within enlarged Diesel injection nozzles (mini-sac and VCO type) was visualised with a high-speed digital video system for various flow conditions and different needle positions. The following observations could be made:

- A vortex flow is formed in the volume between the needle, needle seat and two adjacent holes in both the min-sac and the VCO type nozzles for higher needle lift positions. This vortex structure is a prerequisite for string cavitation to occur.
- Starting from an already cavitating injection hole, a cavitation string can propagate along the low pressure core region of the vortex into the neighbouring hole. There the string tip diffuses into a bubble cloud which initiates hole cavitation.

- ‘Needle strings’ were frequently identified inside the VCO type nozzle at low needle lifts but less frequent at higher needle lifts.
- At higher cavitation numbers, a strong helical movement of the flow structures inside the injection holes of the VCO nozzle was evident occasionally.
- The hole inlet flow around the side corners of an injection hole was identified as a possible mechanism for cavitation initiation.
- The cavitation flow patterns seem to exhibit a more stable structure with increasing needle lift for both nozzle types.
- In the lower nozzle tip volume of both nozzle types, no appreciable liquid movement could be identified.

In order to gain more qualitative information about the correlation between the cavitation structures and the flow turbulence within the model nozzles, the laser Doppler velocimetry technique was applied to obtain the local mean velocity, RMS and turbulent kinetic energy values at numerous locations inside the mini-sac type nozzle. Investigation of the flow field in the sac volume and the injection holes revealed the following:

- The influence of the cavitation phenomenon on turbulence (RMS) levels in the sac volume and in the vicinity of the injection holes is negligible compared to the cavitation influence inside the holes for the investigated flow conditions.
- The recirculation zone close to the hole entrance is reduced in the case of higher needle lift and non-cavitating flow condition. The bulk liquid below the recirculation zone at that location moves with a relatively higher velocity at low needle lifts for the same flow rate.
- An increase in the turbulence levels was identified in the lower part of the injection hole away from the recirculation and cavitation zones with increasing cavitation number at moderate flow rates. This trend is more apparent at the higher needle lift settings.
- At moderate as well as increased flow rates the normalised RMS values are higher at low needle lifts compared to those at high needle lifts due to the bottle neck effect at the needle seat.
- After the onset of cavitation, the recirculation zone in the injection hole is reduced for both low and high needle lifts, which leads to reduced flow restriction. Thus, the bulk velocity below the recirculation zone decreases with higher cavitation number.

- Higher cavitation numbers at increased flow rates result in a more stable and developed flow field with reduced normalised turbulence levels at low needle lifts at all measured positions and for high needle lift towards the hole exit.
- Increasing cavitation and Reynolds numbers results in higher values of the turbulent kinetic energy in the bulk flow below the cavitation and recirculation zones. This increase of turbulent kinetic energy is less apparent as the liquid moves downstream through the injection hole.
- Close to the hole exit the averaged turbulent kinetic energy for all cavitation conditions decreases asymptotically to the turbulence level of the non-cavitating flow.
- This and the theory of turbulent bubble break-up suggest that the break-up process has reduced the initially increased turbulent kinetic energy to the level of the non-cavitating flow condition.

ACKNOWLEDGMENTS

The authors would like to thank Dr. J.M. Nouri for his help with the LDV measurements and Dr. J.S. Shrimpton for making the high-speed video system available.

This research was funded in part by the European Commission in the framework of the Growth Programme (Project Number: GRD1-1999-10034).

REFERENCES

1. Knapp, R.T., J.W. Daily, and F.G. Hammitt, *Cavitation*. 1970, New York; London: McGraw-Hill.
2. Brennen, C.E., *Cavitation and Bubble Dynamic*. 1995, New York; Oxford: Oxford University Press.
3. He, L. and F. Ruiz, *Effect of Cavitation on Flow and Turbulence in Plain Orifice for High-Speed Atomization*. Atomization and Sprays, 1995. **5**(6): p. 569-584.
4. Zhen, H., S. Yiming, S. Shiga, H. Nakamura, and T. Karasawa, *The Orifice Flow Pattern, Pressure Characteristics, and Their Effects on the Atomization of Fuel Containing Dissolved Gas*. Atomization and Sprays, 1994. **4**(2): p. 123-133.
5. Arcoumanis, C. and M. Gavaises, *Linking Nozzle Flow with Spray Characteristics in a Diesel Fuel Injection System*. Atomization and Sprays, 1998. **8**(3): p. 307-347.
6. Arcoumanis, C., M. Gavaises, and V. French, *Effects of Fuel Injection Processes on the Structure of Diesel Sprays*. SAE Paper 970799, 1997.
7. Soteriou, C., M. Smith, and R.J. Andrews, *Diesel Injection - Laser Light Sheet Illumination of the Development of Cavitation in Orifices*. IMechE Paper C529/018/98, 1998.
8. Chaves, H. and F. Obermeier. *Correlation between Light Absorption Signals of Cavitating Nozzle Flow within and outside of the Hole of a Transparent Diesel Injection Nozzle*. in Proc. ILASS-EUROPE. 1998, July 6-8. Manchester, UK.
9. Arcoumanis, C., M. Badami, H. Flora, and M. Gavaises, *Cavitation in Real-Size Multi-Hole Diesel Injector Nozzles*. SAE Paper 2000-01-1249, 2000.
10. Soteriou, C., R.J. Andrews, and M. Smith, *Direct Injection Diesel Sprays and the Effect of Cavitation and Hydraulic Flip on Atomization*. SAE Paper 950080, 1995.
11. Arcoumanis, C., M. Gavaises, J.M. Nouri, E. Abdul-Wahab, and R.W. Horrocks, *Analysis of the Flow in the Nozzle of a Vertical Multi Hole Diesel Engine Injector*. SAE Paper 980811, 1998.
12. Arcoumanis, C. and M. Gavaises. *Cavitation in Diesel Injectors: Modelling and Experiments*. in Proc. ILASS-EUROPE. 1998, July 6-8. Manchester, UK.
13. Arcoumanis, C., J.M. Nouri, and R.J. Andrews. *Application of Refractive Index Matching to a Diesel Nozzle Internal Flow*. in Proc. IMechE Seminar on Diesel Fuel Injection Systems. 1992, April 14-15. London, UK.
14. Arcoumanis, C., H. Flora, M. Gavaises, and N. Kampanis, *Investigation of Cavitation in a Vertical Multi-Hole Injector*. SAE Paper 1999-01-0524, 1999.
15. Arcoumanis, C., M. Gavaises, H. Flora, and H. Roth, *Visualisation of Cavitation in Diesel Engine Injectors*. Mécanique & Industries, 2001. **2**(5): p. 375-381.
16. Afzal, H., *Investigation of Cavitation in Diesel Engine Injectors*. 1999, 4M Final Year Individual Project Report, Mechanical Engineering; Imperial College of Science, Technology and Medicine: London.
17. Kim, J.H., K. Nishida, and H. Hiroyasu. *Characteristics of Internal Flow in a Diesel Injection Nozzle*. in Proc. ICCLASS. 1997, August 18-22. Seul, Korea.
18. Soteriou, C.C.E., M. Smith, and R.J. Andrews, *Cavitation Hydraulic Flip and Atomization in Direct Injection Diesel Sprays*. IMechE Paper C465/051/93, 1993.

19. Soteriou, C., R.J. Andrews, N. Torres, M. Smith, and R. Kunkulagunta. *Through the Diesel Nozzle Hole - A Journey of Discovery II.* in Proc. ILASS-Europe. 2001, September 2-6. Zurich, Switzerland.
20. Afzal, H., C. Arcoumanis, M. Gavaises, and N. Kampanis, *Internal Flow in Diesel Injector Nozzles: Modelling and Experiments.* IMECE Paper S492/S2/99, 1999.
21. Martínez-Bazán, C., J.L. Montanés, and J.C. Lasheras, *On the Breakup of an Air Bubble Injected into a Fully Developed Turbulent Flow. Part 1. Breakup Frequency.* Journal of Fluid Mechanics, 1999. **401**: p. 157-182.
22. Martínez-Bazán, C., J.L. Montanés, and J.C. Lasheras, *On the Breakup of an Air Bubble Injected into a Fully Developed Turbulent Flow. Part 2. Size PDF of the Resulting Daughter Bubbles.* Journal of Fluid Mechanics, 1999. **401**: p. 183-207.
23. Plesset, M.S. and A. Prosperetti, *Bubble Dynamics and Cavitation.* Annual Review of Fluid Mechanics, 1977. **9**: p. 145-185.
24. Plesset, M.S., *The Dynamics of Cavitation Bubbles.* Journal of Applied Mechanics, 1949. **16**: p. 277-282.

CONTACT

Professor C. Arcoumanis, City University, School of Engineering, Northampton Square, London EC1V 0HB, UK
 Tel.: +44-20-7040-0113
 E-mail: C.Arcoumanis@city.ac.uk

NOMENCLATURE

CCD	Charged coupled device
CN	Cavitation number, $CN = \frac{p_{inj} - p_{back}}{p_{back} - p_{vapour}}$
D	Diameter of the injection holes, D = 3.5mm
I	Position of measurement plane from hole inlet
L	Length of the injection hole, L = 12.5mm
LDV	Laser Doppler velocimetry
PAL	Phase alternating line
p _{back}	Back pressure, absolute values
p _{inj}	Injection pressure, absolute values
p _{vapour}	Vapour pressure of the working fluid
r	Position of measurement location from bottom side of hole
Re	Reynolds number, $Re = \frac{U_{inj}D}{v}$
RMS	Root mean square values of the local velocities
TKE	Turbulent kinetic energy, TKE ~ RMS ²
U _{inj}	Mean injection velocity inside the holes obtained from the measured flow rate through the nozzle and the total hole area
v	Local mean velocity assembled from the probability weighted instantaneous velocities at one measurement location
VCO	Valve covering orifice
v	Kinematic viscosity of the working fluid